SCHOOL OF

# NUCLEAR ENGINEERING

COO-2826-10
PNE-78-133



# FAST BREEDER BLANKET FACILITY
Quarterly Progress Report
for the Period July 1, 1978
— September 30, 1978

Edited by
F. M. Clikeman

Prepared for
The U.S. Energy Research and
Development Administration
Under Contract No. EY-76-S-02-2826



September, 1978
Purdue University, West Lafayette, Indiana 47907

## DISCLAIMER

NOTICE

This report was prepared as an account of work sponsored by the United States Government. Neither the United States nor the United States Department of Energy, nor any of their employees, makes any warranty, express or implied, or assumes any legal liability or responsibility for the accuracy, completeness, or usefulness of any information, apparatus, product of process disclosed or represents that its use would not infringe privately owned rights.

ABSTRACT

This quarterly progress report summarizes work done at Purdue University's Fast Breeder Blanket Facility for the Department of Energy during the months July - September 1978. The summary includes reports on the models and methods used to characterize the FBBF facility. Using the reported models and calculational methods and computer codes a new cross section set has been generated, self-shielded for 300° K for use in all FBBF calculations using the 2DB computer code. The summary includes reports of the reproducability of foil activation data and measurements of the azmuthal symmetry of the facility. The status of the development of technique for the experimental measurements and preliminary foil activation measurements are also reviewed.

LIST OF CONTENT

LIST OF FIGURES

LIST OF TABLES

TASK B
(R.C. Borg)

## B.1. Introduction

The object of this task is to perform a detailed preanalysis of the first experimental sequence. The self-shielding factor group constant generation capability was used to obtain a 30 group library. A brief discription of the calculational procedure, modifications to the available computer codes and list of the evaluated self-shielded microscopic and macroscopic group constants is given in Sec. B.2. These macroscopic and microscopic group constants were used for the final preanalysis of the initial loading. The calculational procedure and model are presented in Sec. B.3. Some of the results based on the model of Sec. B.3 and group constants described in B.2 are compared later with the experimental results in Sec. C.3.

## B.2. Group Constant Generation
(R.C. Borg and M.P. Sohn)

Group constants for the FBBF were generated at Argonne National Laboratory based on the Bondarenko self-shielding factor method,[1,2] using the 1DX code.[3] The 50-group, 101-isotope group constant library, LIB-IV,[4] was used as the base library for the calculations.

The card image format of the original base library was processed by the BINX code[5] which converts BCD card images to binary. These binary data files are used by CINX[6] which transforms the CCCC-files[7] (ISOTXS and BROKXS) into the format required for input to the 1DX code. In addition, CINX was also used to reduce the size of the down-scatter band from the original 49 groups, to a more managable 30 groups.

1DX is a one-dimensional diffusion code for generating effective nuclear cross sections. It employs the Bondarenko self-shielding factor method of treating resonance self-shielding. The 1DX code was modified to include an external source option, similar to that used in the 2DB[8] code. The addition of the external source option allowed a multiregion one-dimensional model of the FBBF to be used for calculating the weighting spectrum for the cross section collapse from 50 to 30 groups. The original 50 group and final 30 group energy structures are presented in Tables B.1 and B.2.

The one-dimensional model is shown in Fig. B.1, and is the same as the radial midplane of the two-dimensional model used in earlier pre-analysis calculations.[9] The smeared atom number densities for the materials in each of the six regions are given in Table B.3. In addition, several other homogenized regional materials (material No. 7 to material No. 11),

TABLE B.1

LIB-IV Group Structure

| Group | Max. Energy (eV) | Δu |
|---|---|---|
| 1 | 1.5000E+07 | 0.405 |
| 2 | 1.0000E+07 | 0.5 |
| 3 | 6.0653E+06 | 0.5 |
| 4 | 3.6788E+06 | 0.5 |
| 5 | 2.2313E+06 | 0.5 |
| 6 | 1.3534E+06 | 0.5 |
| 7 | 8.2085E+05 | 0.5 |
| 8 | 4.9787E+05 | 0.25 |
| 9 | 3.8774E+05 | 0.25 |
| 10 | 3.0197E+05 | 0.25 |
| 11 | 2.3518E+05 | 0.25 |
| 12 | 1.8316E+05 | 0.25 |
| 13 | 1.4264E+05 | 0.25 |
| 14 | 1.1109E+05 | 0.25 |
| 15 | 8.6517E+04 | 0.25 |
| 16 | 6.7379E+04 | 0.25 |
| 17 | 5.2475E+04 | 0.25 |
| 18 | 4.0868E+04 | 0.25 |
| 19 | 3.1828E+04 | 0.25 |
| 20 | 2.4788E+04 | 0.25 |
| 21 | 1.9305E+04 | 0.25 |
| 22 | 1.5034E+04 | 0.25 |
| 23 | 1.1709E+04 | 0.25 |
| 24 | 9.1188E+03 | 0.25 |
| 25 | 7.1017E+03 | 0.25 |
| 26 | 5.5308E+03 | 0.25 |
| 27 | 4.3074E+03 | 0.25 |
| 28 | 3.3546E+03 | 0.25 |
| 29 | 2.6126E+03 | 0.25 |
| 30 | 2.0347E+03 | 0.25 |
| 31 | 1.5846E+03 | 0.25 |
| 32 | 1.2341E+03 | 0.25 |
| 33 | 9.6112E+02 | 0.25 |
| 34 | 7.4852E+02 | 0.25 |
| 35 | 5.8295E+02 | 0.25 |
| 36 | 4.5400E+02 | 0.25 |
| 37 | 3.5358E+02 | 0.25 |
| 38 | 2.7536E+02 | 0.5 |
| 39 | 1.6702E+02 | 0.5 |
| 40 | 1.0130E+02 | 0.5 |
| 41 | 6.1442E+01 | 0.5 |
| 42 | 3.7267E+01 | 0.5 |
| 43 | 2.2603E+01 | 0.5 |
| 44 | 1.3710E+01 | 0.5 |
| 45 | 8.3153E+0 | 0.5 |
| 46 | 5.0435E+0 | 0.5 |
| 47 | 3.0590E+0 | 0.5 |
| 48 | 1.8554E+0 | 0.5 |
| 49 | 1.1254E+0 | 0.5 |
| 50 | 6.8256E-1 | 11.31 |

Minimum Energy = 1.0000E-5 eV

TABLE B.2

Group Structure
of
LIB-IV 30 Group Subset

| Group | Max. Energy (eV) | Δu |
|---|---|---|
| 1 | 1.5000E+7 | 0.905 |
| 2 | 6.0653E+6 | 0.5 |
| 3 | 3.6788E+6 | 0.5 |
| 4 | 2.2313E+6 | 0.5 |
| 5 | 1.3534E+6 | 0.5 |
| 6 | 8.2085E+5 | 0.5 |
| 7 | 4.9787E+5 | 0.5 |
| 8 | 3.0197E+5 | 0.5 |
| 9 | 1.8316E+5 | 0.5 |
| 10 | 1.1109E+5 | 0.5 |
| 11 | 6.7379E+4 | 0.5 |
| 12 | 4.0868E+4 | 0.5 |
| 13 | 2.4788E+4 | 0.5 |
| 14 | 1.5034E+4 | 0.5 |
| 15 | 9.1188E+3 | 0.5 |
| 16 | 5.5308E+3 | 0.5 |
| 17 | 3.3546E+3 | 0.5 |
| 18 | 2.0347E+3 | 0.5 |
| 19 | 1.2341E+3 | 0.5 |
| 20 | 7.4852E+2 | 0.5 |
| 21 | 4.5400E+2 | 0.5 |
| 22 | 2.7536E+2 | 0.5 |
| 23 | 1.6702E+2 | 0.5 |
| 24 | 1.0130E+2 | 0.5 |
| 25 | 6.1442E+1 | 0.5 |
| 26 | 3.7267E+1 | 0.5 |
| 27 | 1.3710E+1 | 0.5 |
| 28 | 5.0435E+0 | 0.5 |
| 29 | 1.8554E+0 | 0.5 |
| 30 | 6.8256E-1 | 11.31 |

Minimum Energy = 1.0000E-5 eV

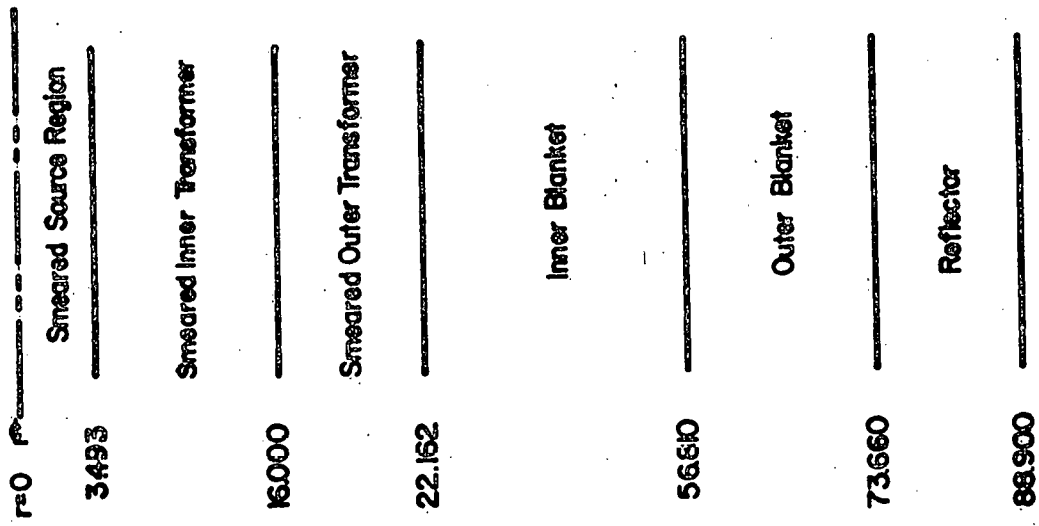


Figure B.1: 6 Region One-Dimensional Model
(dimensions in cm)

TABLE B.3

Region and Material Description
for which Macroscopic Group
Constants are available
(atom/barn · cm)

Material 1 (Source Region)

| | |
|---|---|
| Fe | 3.97923E-2 |
| Cr | 1.15824E-2 |
| Ni | 5.71652E-3 |
| Mn | 9166026E-3 |
| Mo | 1.59201E-4 |

Material 2 (Inner Trans.)

| | |
|---|---|
| Fe | 8.85800E-3 |
| Cr | 2.43116E-3 |
| Ni | 1.45338E-3 |
| Mn | 1.53952E-4 |
| Mo | 1.60214E-4 |
| C | 2.89698E-3 |
| B10 | 2.29454E-3 |
| B11 | 9.29372E-3 |
| U35 | 7.19192E-4 |
| U38 | 1.42640E-2 |
| O | 2.99663E-2 |

Material 3 (Outer Trans.)

| | |
|---|---|
| Fe | 9.75225E-3 |
| Cr | 2.81526E-3 |
| Ni | 1.42987E-3 |
| Mn | 2.47970E-4 |
| Mo | 5.89391E-5 |
| C | 3.24765E-3 |
| B10 | 2.57213E-3 |
| B11 | 1.04185E-2 |
| U35 | 2.64600E-4 |
| U38 | 5.24805E-3 |
| O | 1.10253E-2 |
| Na | 8.04813E-3 |

Material 4 (Inner Blanket)

| | |
|---|---|
| Fe | 9.75555E-3 |
| Cr | 2.63892E-3 |
| Ni | 1.64975E-3 |
| Mn | 1.46918E-4 |
| Mo | 2.10324E-4 |
| Al | 7.15459E-3 |
| U35 | 1.01846E-4 |
| U38 | 1.40575E-2 |
| O | 2.83188E-2 |

Material 5 (Outer Blanket)
Al-secon clad

| | |
|---|---|
| Al | 1.75838E-2 |
| U35 | 1.01844E-4 |
| U38 | 1.40573E-2 |
| O | 2.83182E-2 |

Material 6 (Reflector)

| | |
|---|---|
| Fe | 4.09061E-2 |
| C | 3.82887E-4 |
| Mn | 1.88348E-4 |
| Na | 5.96336E-3 |

Material 7 (I.T. Pin Ends)

| | |
|---|---|
| Fe | 8.82571E-3 |
| Cr | 6.12504E-3 |
| Ni | 3.17902E-3 |
| Mn | 5.22776E-4 |
| Mo | 1.60214E-4 |
| C | 2.89698E-3 |
| B10 | 2.29454E-3 |
| B11 | 9.29372E-3 |

Material 8 (O.T. Pin Ends)

| | |
|---|---|
| Fe | 1.43577E-2 |
| Cr | 4.17734E-3 |
| Ni | 2.06478E-3 |
| Mn | 3.83669E-4 |
| Mo | 5.89391E-5 |
| C | 3.24765E-3 |
| B10 | 2.57213E-3 |
| B11 | 1.04185E-2 |
| Na | 8.04813E-3 |

Material 9 (Top Plug)

| | |
|---|---|
| Fe | 5.76672E-2 |
| Cr | 1.70555E-2 |
| Ni | 7.95001E-3 |
| Mn | 1.69917E-3 |

Material 10 (Bottom Plug)

| | |
|---|---|
| Fe | 1.90601E-2 |
| Cr | 5.63715E-3 |
| Ni | 2.62763E-3 |
| Mn | 5.61607E-4 |

Material 11 (Base Plate)

| | |
|---|---|
| Fe | 8.30325E-2 |
| C | 7.77196E-4 |
| Mn | 3.82314E-4 |

necessary for the two-dimenisonal calculations, are presented in Table B.3. They are the materials used in non-midplane regions. The weighting functions used in the collapsing of the macroscopic group constants are identified in Table B.4 for each of the materials. A number of foil materials were also processed for both the inner and outer blanket regions. A list is given in Table B.5. The available 30 group microscopic cross sections from the 1DX calculations are indicated in Table B.6.

TABLE B.4

Macroscopic Group Constant
Weighting Function Designation

| | Material Description | Weighting Function |
|---|---|---|
| 1. | Homogenized Source Region | Source Region Flux |
| 2. | Inner Transformer Region | Inner Transformer |
| 3. | Outer Transformer Region | Outer Transformer |
| 4. | Inner Blanket Region | Inner Blanket |
| 5. | Outer Blanket Region | Outer Blanket |
| 6. | Reflector Region | Reflector |
| 7. | Non-active Inner Transformer | Inner Transformer |
| 8. | Non-active Outer Transformer | Outer Transformer |
| 9. | Top Source Plug | Source |
| 10. | Bottom Source Plug | Source |
| 11. | Steel Base Plate | Inner Blanket |

TABLE B.5

Activation foil materials
for Inner and Outer Blanket

Mg

Ti

Co-59

Cu-63

Ag-109

Dy-164

Ta-181

W-182

W-183

W-184

W-186

Au 197

Th-232

Np-237

Pu-239

TABLE B.6

Material for which Microscopic Group Constants are Available Including Region Flux Weighting

Microscopic Cross Sections

| Material Regions | Source | I.T. | O.T. | I.B. | O.B. | Reflector |
|---|---|---|---|---|---|---|
| Fe | ✓ | ✓ | ✓ | ✓ | | ✓ |
| Cr | ✓ | ✓ | ✓ | ✓ | | |
| Ni | ✓ | ✓ | ✓ | ✓ | | |
| Mn | ✓ | ✓ | ✓ | ✓ | | ✓ |
| Mo | ✓ | ✓ | ✓ | ✓ | | |
| C | | ✓ | ✓ | | | ✓ |
| B-10 | | ✓ | ✓ | | | |
| B-11 | | ✓ | ✓ | | | |
| U-235 | | ✓ | ✓ | ✓ | ✓ | |
| U-238 | | ✓ | ✓ | ✓ | ✓ | |
| O | | ✓ | ✓ | ✓ | ✓ | |
| Na | | | ✓ | | | ✓ |
| Al | | | | ✓ | ✓ | |
| Mg | | | | ✓ | ✓ | |
| Ti | | | | ✓ | ✓ | |
| Co-59 | | | | ✓ | ✓ | |
| Cu-63 | | | | ✓ | ✓ | |
| Ag-109 | | | | ✓ | ✓ | |
| Dy-164 | | | | ✓ | ✓ | |
| Ta-181 | | | | ✓ | ✓ | |
| W-182 | | | | ✓ | ✓ | |
| W-183 | | | | ✓ | ✓ | |
| W-184 | | | | ✓ | ✓ | |
| W-186 | | | | ✓ | ✓ | |
| Au-197 | | | | ✓ | ✓ | |
| Th-232 | | | | ✓ | ✓ | |
| Np-237 | | | | ✓ | ✓ | |
| Pu-239 | | | | ✓ | ✓ | |

## B.3. Description of Preanalysis Calculational Model (M.P. Sohn and R.C. Borg)

The calculational model has remained essentially unchanged since its original presentation in Ref. 9. Only the radius of the inner blanket/outer blanket interface has been changed to correspond to actual dimensions of these blanket regions. The details of the calculational model are presented in Fig. B.2 with material and volume fraction specifications given in Tables B.7 and B.8. In addition, the neutron source distribution of the $^{252}Cf$ source is presented in Table B.9.

The 2DB code was used to calculate the flux based on the model described in the previous paragraph and the group constants described in Sec. B.2. A number of auxilary programs have been written to perform the reaction rate calculations based on the 2DB flux. The most important were used to obtain the results compared in Sec. C.3. They include the following:

RRATE -- A program to calculate reaction rates using the 2DB flux dump and physical model.

RRPLOT -- A program to plot total reaction rates or fluxes as a function of radial or axial position.

SPCPLOT -- A program to plot energy spectra of either fluxes or reaction rates.

All of these programs are operational and users manuals are currently being prepared.

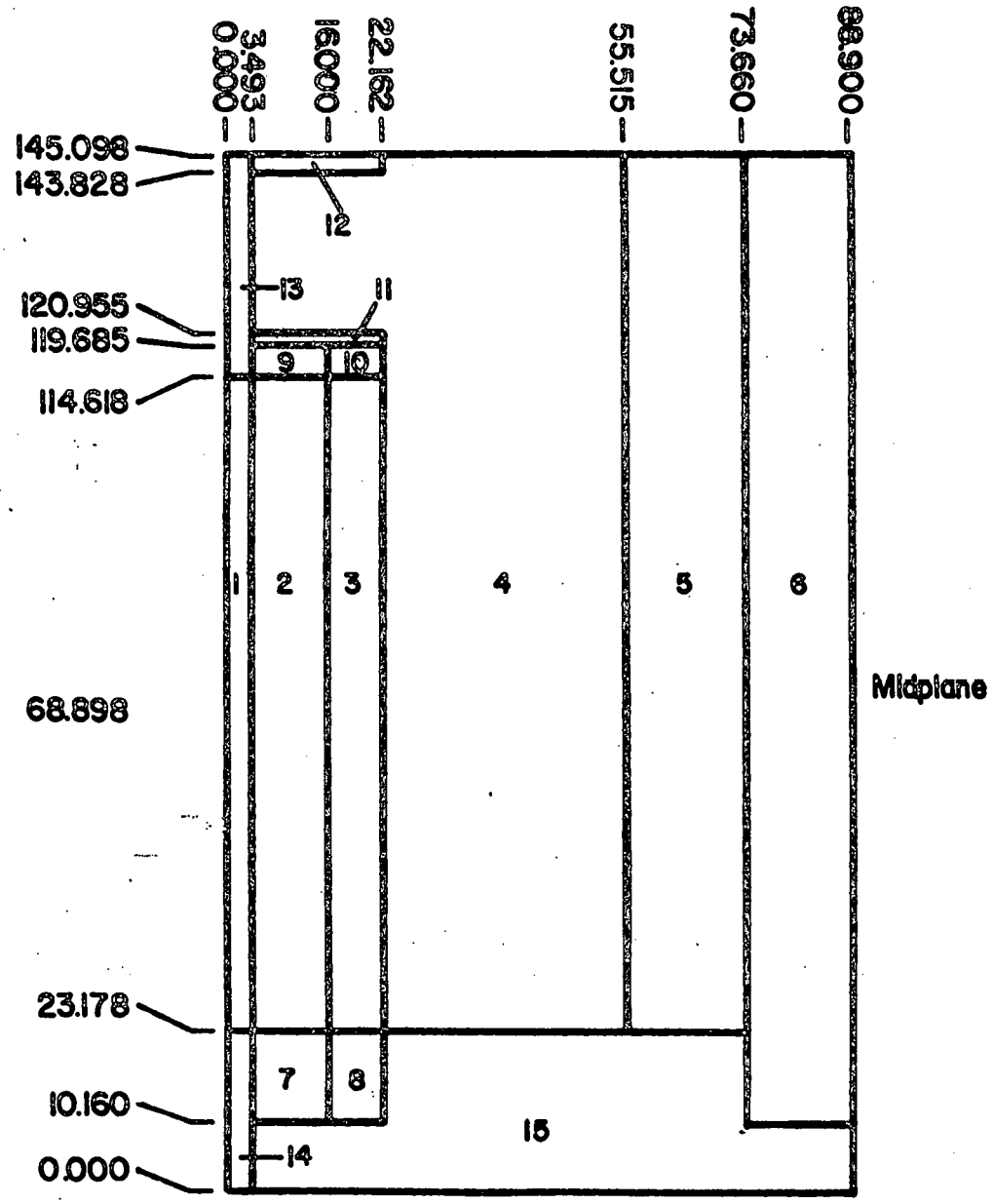


Figure B.2: Two-Dimensional Model of FBBF (all dimensions in cm).

TABLE B.7

Volume Fractions for Two-Dimensional Model

| Region Number | Region | Material | Volume Fraction |
|---|---|---|---|
| 1 | Smeared Source Region | SS-316 | 0.130896 |
| | | SS-304 | 0.561983 |
| 2 | Smeared Inner Transformer | SS-304 | 0.024740 |
| | | SS-316 | 0.131729 |
| | | $B_4C$ (0.612 T.D.) | 0.172224 |
| | | 4.8% $UO_2$ | 0.651182 |
| 3 | Smeared Outer Transformer | SS-304 | 0.121706 |
| | | SS-316 | 0.048460 |
| | | $B_4C$ (0.538 T.D) | 0.220681 |
| | | 4.8% $UO_2$ | 0.239585 |
| | | Na | 0.345058 |
| 4 | Inner Blanket | SS-316 | 0.172929 |
| | | Al | 0.118628 |
| | | Nat $UO_2$ | 0.615044 |
| 5 | Outer Blanket | Al | 0.291552 |
| | | Nat $UO_2$ | 0.615032 |
| 6 | Reflector | C-Steel | 0.492652 |
| | | Na | 0.234680 |
| 7 and 9 | Non-active Inner Transformer | SS-304 | 0.206102 |
| | | SS-316 | 0.131713 |
| | | $B_4C$ (0.612 T.D.) | 0.172224 |
| 8 and 10 | Non-active Outer Transformer | SS-304 | 0.206102 |
| | | SS-316 | 0.048461 |
| | | $B_4C$ (0.538 T.D.) | 0.206293 |
| | | Na | 0.354901 |
| 11 and 12 | Axial Blanket Steel Plates | C-Steel | 1.000 |
| 13 | Top Plug (Source Region) | SS-304 | 1.000 |
| 14 | Bottom Plug (Source Region) | SS-304 | 0.330518 |
| 15 | Carbon Steel Base | C-Steel | 1.000 |

The remainder of each region is void.

TABLE B.8

Number Densities (atoms/barn · cm)

SS-304 (density - 7.75 gm/cc, Fe - 69% MN - 2%, Cr - 19%, Ni - 10%)

| | |
|---|---|
| Fe | 5.766724E-2 |
| Cr | 1.705547E-2 |
| Ni | 7.950014E-3 |

SS-316 (density - 7.90 gm/cc, Fe - 70.8% Ni - 12%, Cr - 17%, Mn - 1%, Mo - 2.5%)

| | |
|---|---|
| Fe | 5.641361E-2 |
| Cr | 1.526015E-2 |
| Ni | 9.540016E-3 |
| Mn | 8.495855E-4 |
| Mo | 1.216243E-3 |

$B_4C$ (61.2% T.D. in IT)

| | |
|---|---|
| $^{12}C$ | 1.682100E-2 |
| $^{10}B$ | 1.332300E-2 |
| $^{11}B$ | 5.396300E-3 |

$B_4C$ (53.8% T.D. in OT)

| | |
|---|---|
| $^{12}C$ | 1.475650E-2 |
| $^{10}B$ | 1.165540E-2 |
| $^{11}B$ | 4.721050E-3 |

$B_4C$ (60.0% T.D.)

| | |
|---|---|
| $^{12}C$ | 1.647969E-2 |
| $^{10}B$ | 1.305192E-2 |
| $^{11}B$ | 5.286686E-3 |

Nat. $UO_2$ fuel 0.94 T.D.

| | |
|---|---|
| $^{235}U$ | 1.655909E-4 |
| $^{238}U$ | 2.285615E-2 |
| $^{16}O$ | 4.604347E-2 |

4.8% Enriched $UO_2$ fuel 0.94 T.D.

| | |
|---|---|
| $^{235}U$ | 1.104441E-3 |
| $^{238}U$ | 1.104441E-3 |
| $^{16}O$ | 4.601838E-2 |

Carbon Steel (1020, density - 7.75 gm/cc 0.2% C, 0.45% Mn)

| | |
|---|---|
| Fe | 8.303247E-2 |
| C | 7.771964E-4 |
| Mn | 3.823135E-4 |

Aluminum (density - 2.702 gm/cc)

| | |
|---|---|
| $^{25}Al$ | 6.031114E-2 |

Sodium (in OT)

| | |
|---|---|
| $^{23}Na$ | 2.332400E-2 |

Sodium (in Reflector)

| | |
|---|---|
| $^{23}Na$ | 2.541059E-2 |

TABLE B.9

Neutron Distribution of the $^{252}Cf$ 30 Group Source

| Group | Chi |
|---|---|
| 1 | 3.59360E-2 |
| 2 | 1.22967E-1 |
| 3 | 2.11181E-1 |
| 4 | 2.21992E-1 |
| 5 | 1.71446E-1 |
| 6 | 1.09381E-1 |
| 7 | 6.20554E-2 |
| 8 | 3.27682E-2 |
| 9 | 1.65629E-2 |
| 10 | 8.15209E-3 |
| 11 | 3.94806E-3 |
| 12 | 1.89338E-3 |
| 13 | 9.02621E-4 |
| 14 | 4.28750E-4 |
| 15 | 2.03213E-4 |
| 16 | 9.61880E-5 |
| 17 | 4.54925E-5 |
| 18 | 2.15054E-5 |
| 19 | 1.01631E-5 |
| 20 | 4.80202E-6 |
| 21 | 2.26870E-6 |
| 22 | 1.07177E-6 |
| 23 | 5.06297E-7 |
| 24 | 2.39167E-7 |
| 25 | 1.12977E-7 |
| 26 | 7.85764E-8 |
| 27 | 1.75330E-8 |
| 28 | 3.91215E-9 |
| 29 | 8.72921E-10 |
| 30 | 2.50582E-10 |

Normalized to $\sum_{i=1}^{30} \chi_i = 1.00$

TASK C
(F.M. Clikeman)

Introduction

The objectives of this task are: 1) The testing of experimental equipment and the development of techniques for making experimental measurements in the blanket region of the FBBF facility; 2) Performing check-out tests and preparing the operating procedures required for licensing purposes and for the safe operation of the FBBF facility; 3) Performing measurements on the first blanket configuration of the FBBF. Progress of these tasks are summarized in the following section.

## C.1. Testing of Experimental Equipment and Techniques
(F.M. Clikeman)

Testing of the equipment and techniques used for neutron spectroscopy, integral neutron capture rate, fission rate and gamma dosimetry measurements continued during the quarter. Preliminary activation measurements to determine the characteristics of the facility were made and are reported in Sections C.2 and C.3.

### C.1.1 Foil Activation Measurments
(G.A. Harms and F.M. Clikeman)

Preliminary activation of several possible activation foils have been made to determine the gamma-ray spectra and optimum irradiation and counting times for use in the FBBF facility. Samples, usually metallic foils, of the target nuclide are irradiated in several radial positions in the FBBF and then the gamma-ray spectrum analyzed using the Ge(Li) spectrometer system. The spectra are analyzed for the expected gamma rays from the $(n,\gamma)$ reactions in the target nuclide as well as any other possible interfering gamma rays from other nuclides or other reactions such as (n,p). Half lives of the radioisotopes are also usually checked. If no interfering activities are present, the radionuclides will also be counted using a well-type NaI(Tℓ) scintillation detector to increase the detection sensitivity and thereby improve the counting statistics. In one case, $^{198}Au$, the counting efficiency was increased a factor of 15, permitting the measurement of the activity with less than a one percent uncertainty in $10^3$ seconds with the scintillation spectrometer as compared to about four hours with the Ge(Li) detector. Relative radial activation measurements are then made using the scintillation detector with one foil used for repeated measurements to perform chi-squared checks on the detector system. The foil used for the chi-squared test is then also counted using the Ge(Li) spectrometer to determine its absolute activity. The efficiency of the Ge(Li) spectrometer system is determined using an NBS mixed nuclide point source.

The use of the scintillation detector is not applicable in all cases, especially if the target nuclide is radioactive such as $^{238}U$ and $^{232}Th$. In these cases the Ge(Li) spectrometer must be used for the complete analysis.

After the best detection system has been determined, the optimum irradiation and analyzing times are determined, keeping in mind the half lives and level of interfering activities, as well as optimum use of the FBBF facility. From this information, schedules for activation measurements in the FBBF are developed to best coordinate the use of the FBBF and the data acquisition systems.

### C.1.2 Proton-Recoil Proportional Counter Measurements (D.W. Vehar and F.M. Clikeman)

During the progress period detector calibration runs using the PUR-I reactor were completed and the spectroscopy system was moved to the FBBF laboratory. The calibration measurements using the reactor were somewhat inconclusive due to the high gamma ray to fast neutron ratio that exists in the experimental areas of the reactor. However, the techniques that were developed are expected to be applicable with the detector in the FBBF and the calibration of the spectrometer system in the FBBF is now under way.

Following the move to the FBBF laboratory, the optimum electronic configuration and settings for the proton-recoil spectrometer were determined, with respect to energy and rise time analysis of the recoil pulses. Since these settings are dependent on the count rate as well as on the relative intensities of the neutron and gamma radiation, this optimization must be performed for each detector location in the FBBF blanket.

Rise-time distributions of several recoil-proton energies are shown in the following figures. Figures C.1-3 are rise-time distributions corresponding to deposited energies of 20, 30, and 50 keV, respectively, obtained with the eight-atomosphere hydrogen detector at location E-4 in the FBBF blanket. The peak (at channels 36-37) in the rise-time distribution is produced by the neutron events while the distribution at the lower channels, corresponding to long rise-times, is caused by both gamma-ray and neutron events, (note that rise-time is inversely proportional to the channel number in these plots). Figure C.4 shows the corresponding

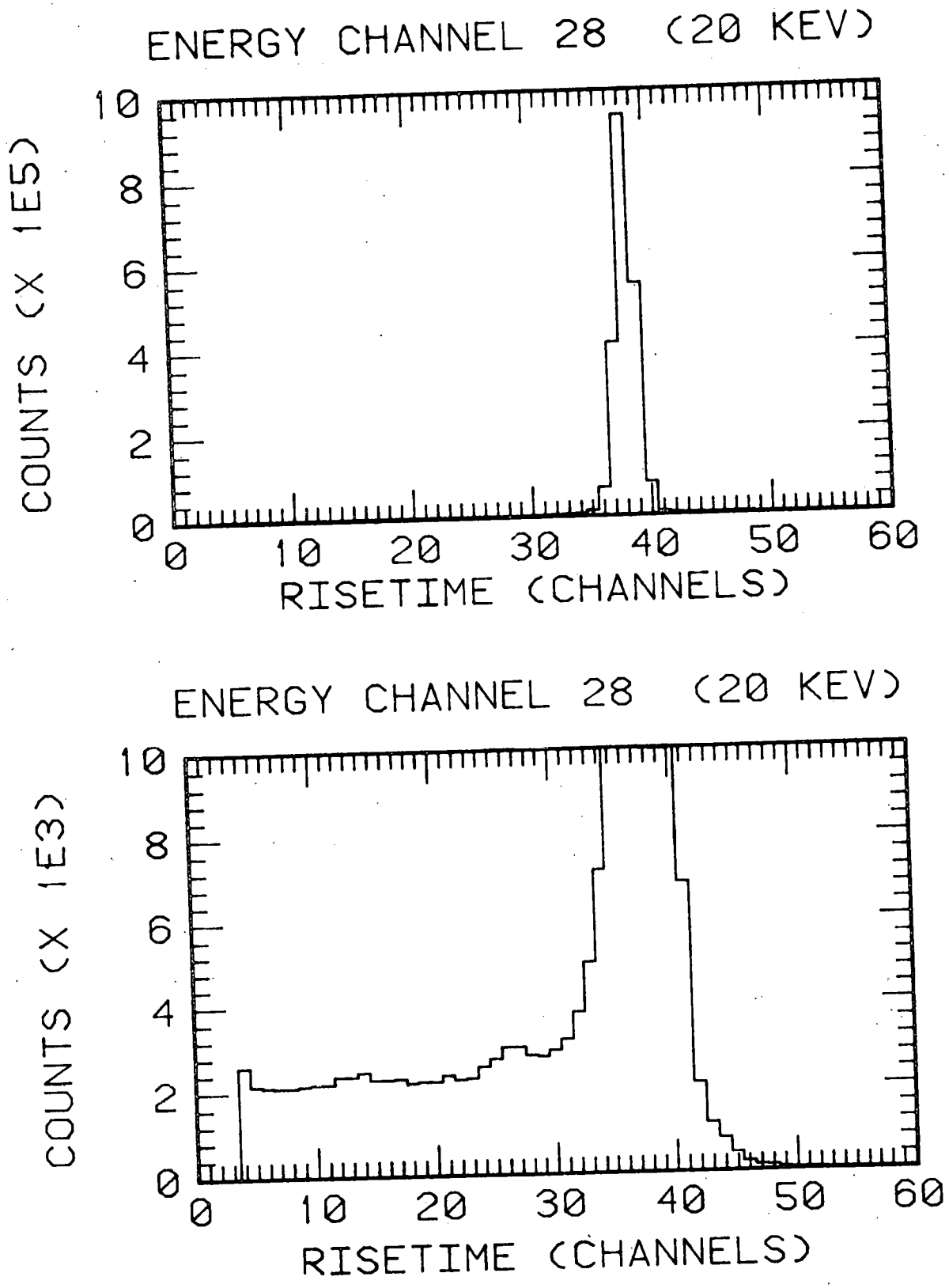


Figure C.1: Rise-time distribution at 20 keV for a mixed neutron and gamma-ray field.

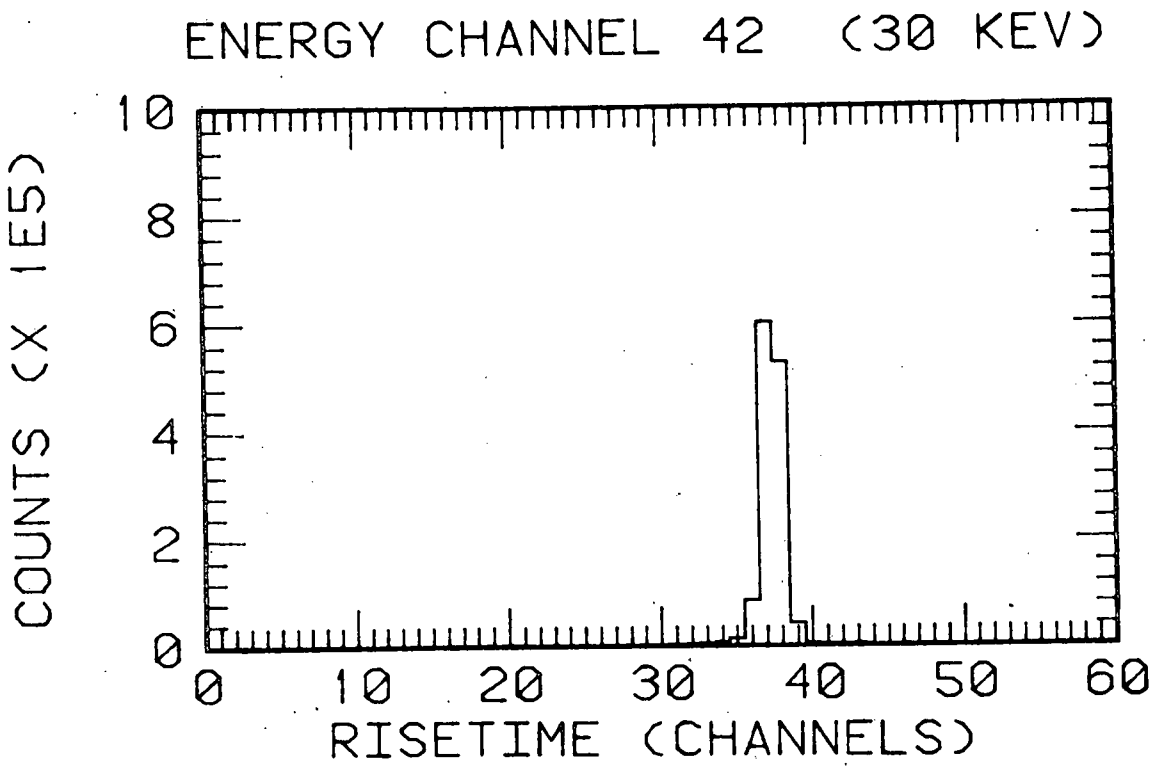


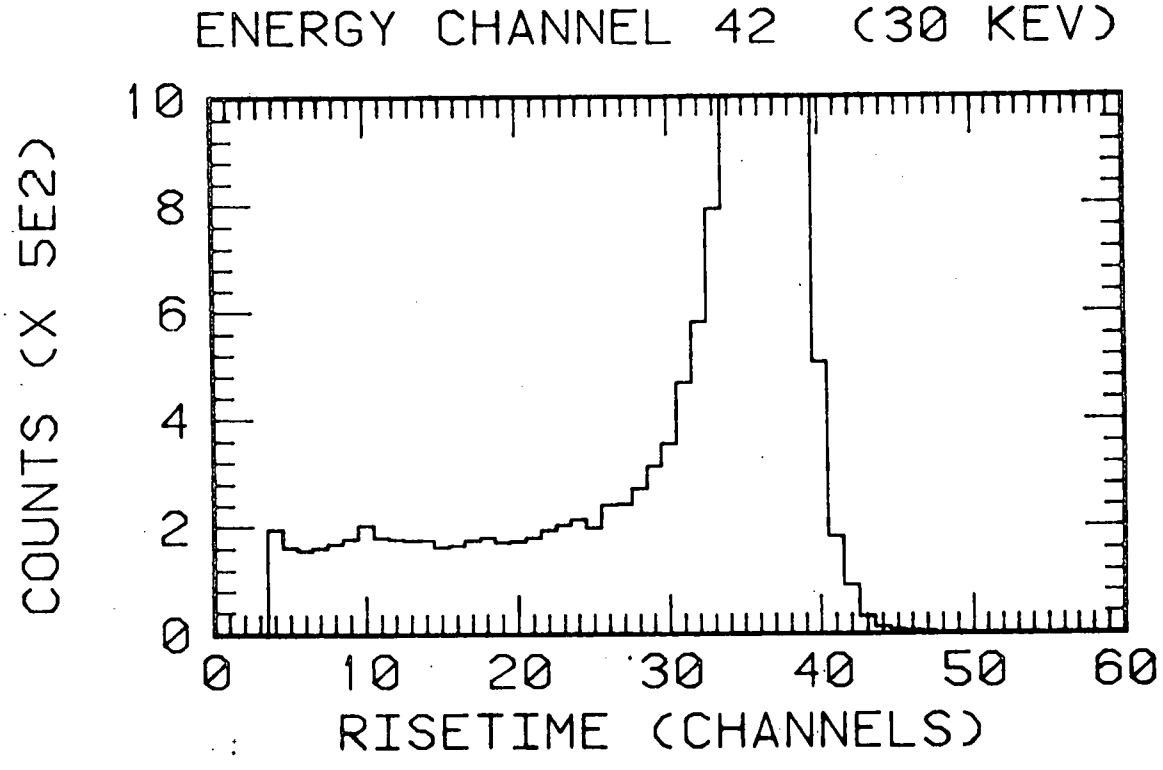


Figure C.2: Rise-time distribution at 30 keV for a mixed neutron and gamma-ray field.

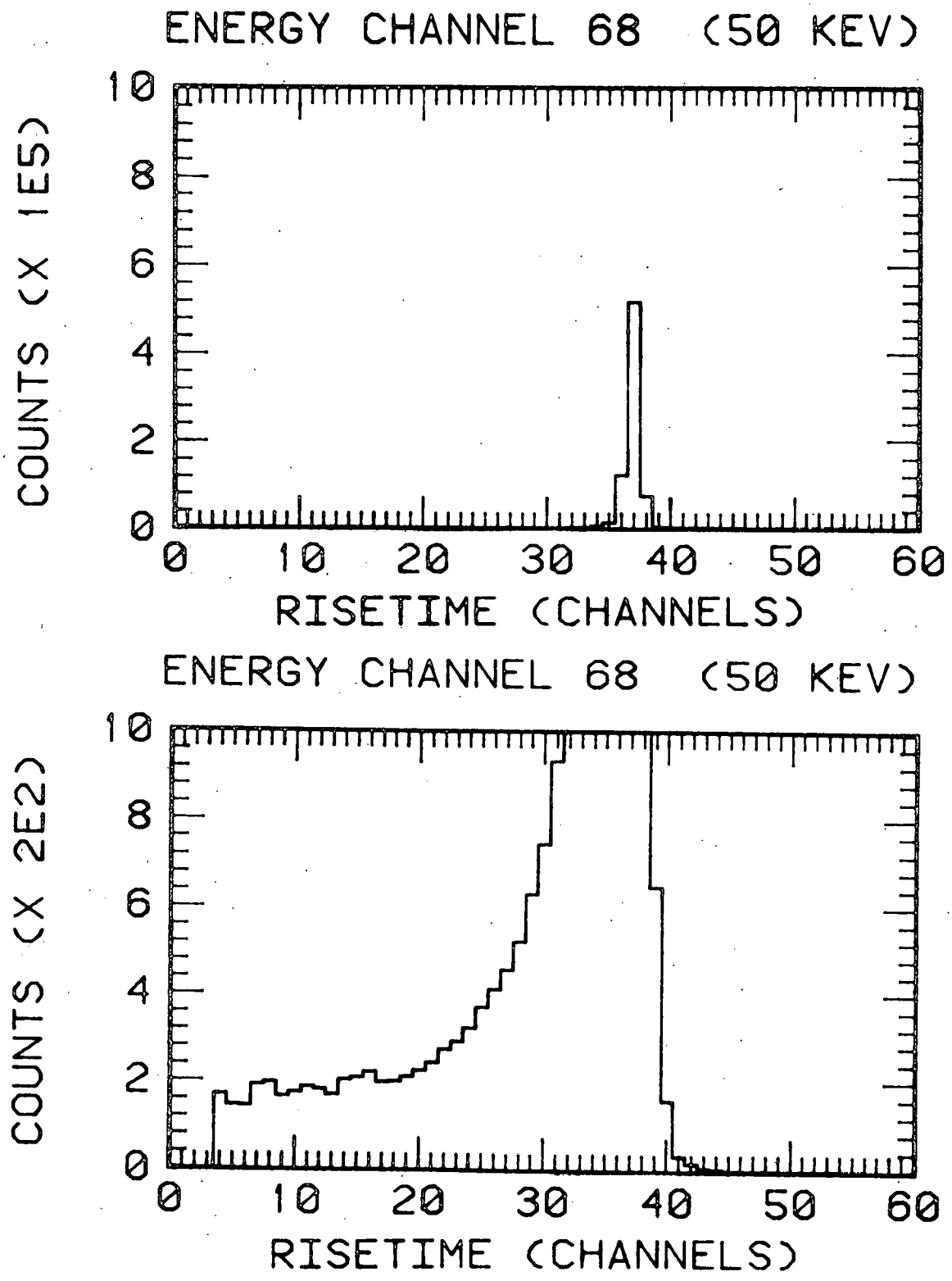


Figure C.3: Rise-time distribution at 50 keV for a mixed neutron and gamma-ray field.

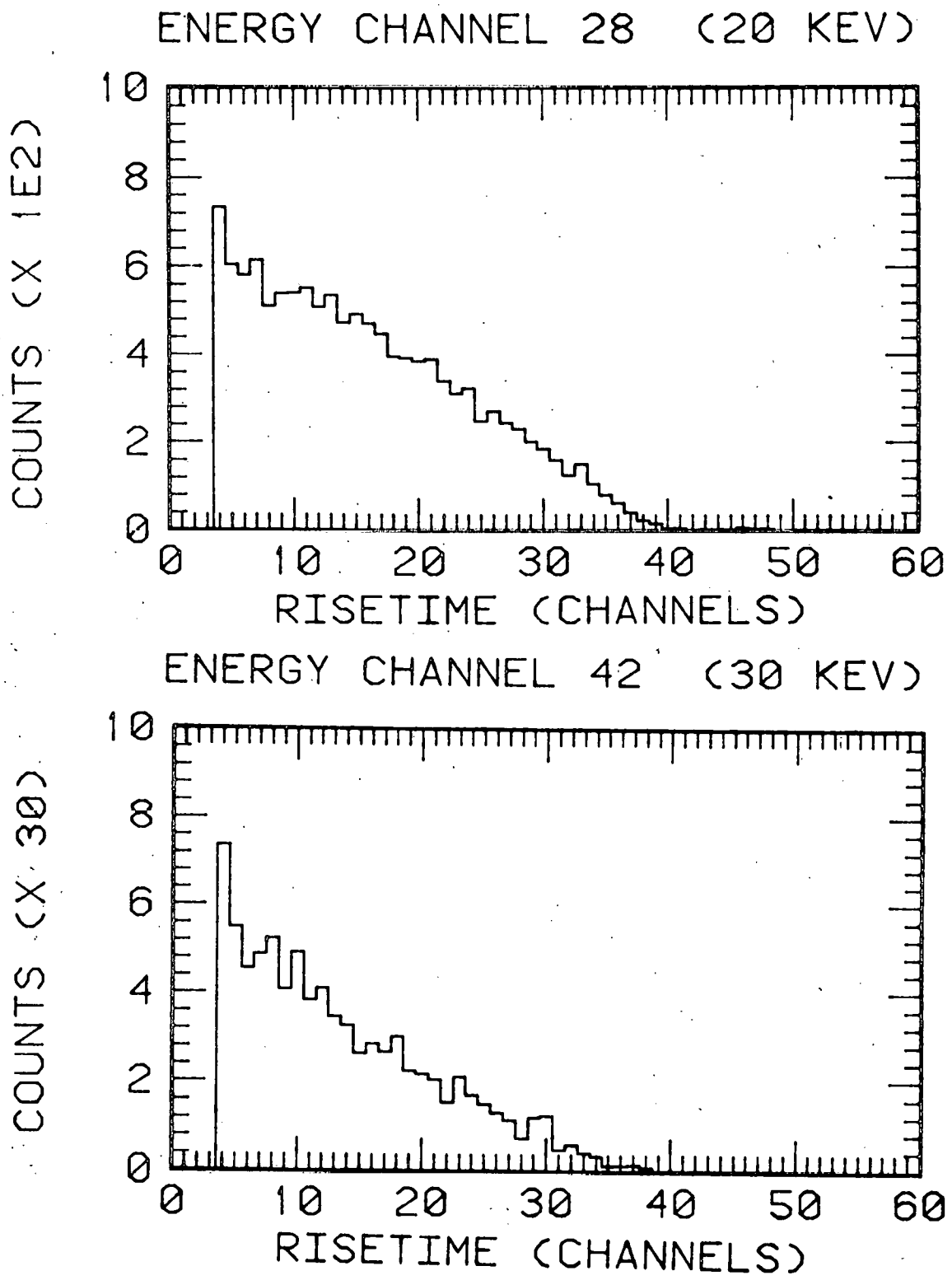


Figure C.4: Rise-time distributions at 20 and 30 keV for a pure gamma (Co-60) source.

rise-time distributions for deposited energy of 20 and 30 keV obtained with a pure gamma (Co-60) source. A rise-time distribution at 50 keV is not presented for the gamma source because the number of counts recorded at that energy was not significant. This is in agreement with the expectation that there should be no gamma-ray events above about 40 keV for this detector. Note also the change of scale in these plots. Two important points are shown on these plots; first the number of gamma-ray events is small compared to the number of proton recoils, even at low energies. This will facilitate the gamma-ray subtraction process. Second, the shapes of the various gamma-ray distributions do not match the shapes of the corresponding neutron + gamma-ray distributions below the proton-recoil peak. This is due to the difference in counting rates for the two cases and to the distortion of proton-recoil pulses, which appear as gamma-ray induced events. In addition, the gamma-ray rise-time distribution is not constant with energy. As a result gamma-ray background removal can not be accomplished by subtracting a previously determined rise-time distribution. Additional work is necessary to determine the best method for subtraction of the gamma-ray events.

Preliminary spectra have been obtained over a limited energy range. The results of two separate runs under the same conditions indicate that reproducible spectra can be obtained. The results also showed that excellent counting statistics can be achieved in reasonable time periods and that the stability of electronics in the analysis system is more than adequate for measurements extending for as long as twenty-four hours.

For a complete neutron-energy spectrum in a range of 1 keV to 2 MeV, it will be necessary to use eight detector voltages: five for the lower energy detector (1 to 150 keV) and three for the upper energy detector

(200 keV to 2 MeV). The data analysis codes are presently written to accept up to eight voltage sets. It is expected that three to four days will be required to accummulate the data for a complete spectrum at one experimental position. It may be better, however, to use a third neutron detector to provide a greater overlap between the regions covered by each detector. The use of the third detector will increase the data acquisition time slightly, but may provide better detector resolution in the important regions near 100 keV.

### C.1.3 Fission Rate Measurements
(H.P. Chou, R.H. Johnson, and F.M. Clikeman)

During the quarter preliminary solid state fission track recorder measurements (SSTR) were made in the blanket regions of the FBBF facility to estimate the irradiation time necessary to obtain adequate counting statistics. Plated thin fission foils (uranium-235 and uranium-238) and round glass disks were sandwiched together in stainless steel and lead capsules and inserted into the experimental fuel rods. Measurements were made at a height corresponding to the midplane of the neutron sources. It was found that in order to get the desired $10^4$ fission tracks on a track recorder, in the region of the blanket-reflector interface, an irradiation time of about two weeks was required for the U-235 foil and for about 1,000 tracks for the U-238 foil about a month was required. In order to speed up the data collection time for the threshold fission foils in the outer blanket regions, thick fission foils were tried. The thick fission foil is considerably thicker than the range of the fission products in the foil material, however, a constant correction factor for the percentage of the fission fragments escaping can be determined by comparing the fission rates for thick and thin foils in the inner region of the FBBF facility where adequate counting statistics can be achieved in reasonably short periods of time. Preliminary experiments using a thick, four hundred PPM depleted uranium foil in the regions of the outer blanket of the FBBF facility indicated that $10^4$ fission tracks can be recorded in a two week radiation period.

Experiments using fused-quartz track recorders were also conducted during the period. Fused-quartz has the same advantages, namely low

background track and sharp image contrast as glass, but in addition gives a higher track registration efficiency. The itching and handling procedures for the fused-quartz are the same as for the glass track recorders.

Work has also progressed on the automatic track counting system. This system couples a traveling optical microscope with a microcomputer. A program for counting the tracks automatically has been implemented and is now being tested. The program determines both the number of tracks and the distribution of the track size. The overlapping of tracks can then be corrected on the basis of the size distribution. In addition, the program can also give information on the position of the tracks on the track recorder which can be used for determination of the spatial distribution of the fission tracks. This information will be useful in the study of the heterogeneity effects in the fuel rods. The analyzing program is coded in machine language and the analyzing time is mainly limited by the scanning time of the microscope. At the present time it takes about four hours to scan a 7 mm x 7 mm square. The program has been tested using the dummy pattern and at the present time testing using actual track recorders is under way.

Until the automatic system is fully operational, the recorders are being counted by hand using photographs taken with a microscope. This procedure gives information required for planning future experiments as well as standard track recorders to be used in checking the automatic counting system.

C.1.4. Gamma-Ray Dosimetry Measurements and Calculations
(K.R. Koch, F.M. Clikeman, R.H. Johnson, J.H. Paczolt)

Gamma-ray heating rate measurements are being made in the FBBF using $CaF_2$:Dy thermoluminescent dosimeters (TLD's). The TLD's being used were previously grouped into "precision sets" for better accuracy.[10] TLD irradiations have been performed for the neutron source down to determine the background due to the natural activity of the fuel. Preliminary measurements were made using 1.80 $g/cm^2$ thick lead holders (sleeves); each holder contained four 3.18 mm x 3.18 mm x 0.89 mm $CaF_2$:Dy chips arranged so that the overall dimensions of the TLD material are 6.35 mm x 6.35 mm x 0.89 mm. Several corrections to the measurements are necessary. First, TLD's from the same precision set (having approximately the same correction factor) were used in each sleeve. By applying correction factors and by averaging the four results of each holder, measurements with a precision of approximately $\pm$1% (one standard deviation) can be obtained. Corrections for the gamma-ray attenuation in the sleeve and for the neutron dose contributions have not yet been made. Similar measurements of the natural background using stainless steel sleeves together with preliminary measurements with the source up are underway.

Solid state ionization theory, "cavity" theory, is being used to correct for the different electron spectra produced in the sleeves and the TLD. The correction is applied as an "f-factor" which is defined as the ratio of the dose in the TLD to the sleeve dose. This allows for dose determination in the sleeve material. F-factors as a function of

gamma-ray energy were obtained from Simons for a single TLD in either stainless steel or lead sleeves;[11] these f-factors were calculated using the TERC/III code.[12] Slightly different f-factors are needed for the actual experimental geometry (four TLD chips per sleeve) because of a slightly higher ratio of volume to surface area. The one and four chip energy-dependent f-factors being used are shown in Fig. C.5.

An average f-factor is calculated for each radial position using the energy absorption coefficients shown in Fig. C.6 and the calculated gamma-ray energy spectrum. The properly weighted f-factor at each spatial point is given in Ref. 12 as

$$f(\vec{r}) = \frac{\int_0^\infty dT_\gamma T_\gamma \phi(\vec{r},T_\gamma) \left[\frac{\mu_{en}(T_\gamma)}{\rho}\right]_{sleeve} f(T_\gamma)}{\int_0^\infty dT_\gamma T_\gamma \phi(\vec{r},T) \left[\frac{\mu_{en}(T_\gamma)}{\rho}\right]_{sleeve}}$$

Preliminary gamma-ray energy spectrum calculations for the FBBF blankets have been performed using the ANISN-W code with a 23 neutron group, 21 gamma-ray group cross section set.[13] Figure C.7 shows energy spectra at two different radii; 40.3 cm is near the middle of the inner blanket and 64.1 cm is near the middle of the outer blanket. The gamma-ray production cross sections in these preliminary calculations were not self-shielded, therefore, new calculations are underway in which the gamma-ray production cross sections for $^{238}U$ are self-shielded. Although self-shielding will reduce the magnitudes of the gamma-ray spectra, it is not expected to significantly change the shapes of the gamma-ray spectra. Thus, the preliminary spectrum calculations should be sufficient

for weighting the f-factors, although self-shielded gamma-ray spectrum calculations will be required with the appropriate kerma factors to obtain the calculated gamma-ray heating rates in lead and stainless steel.

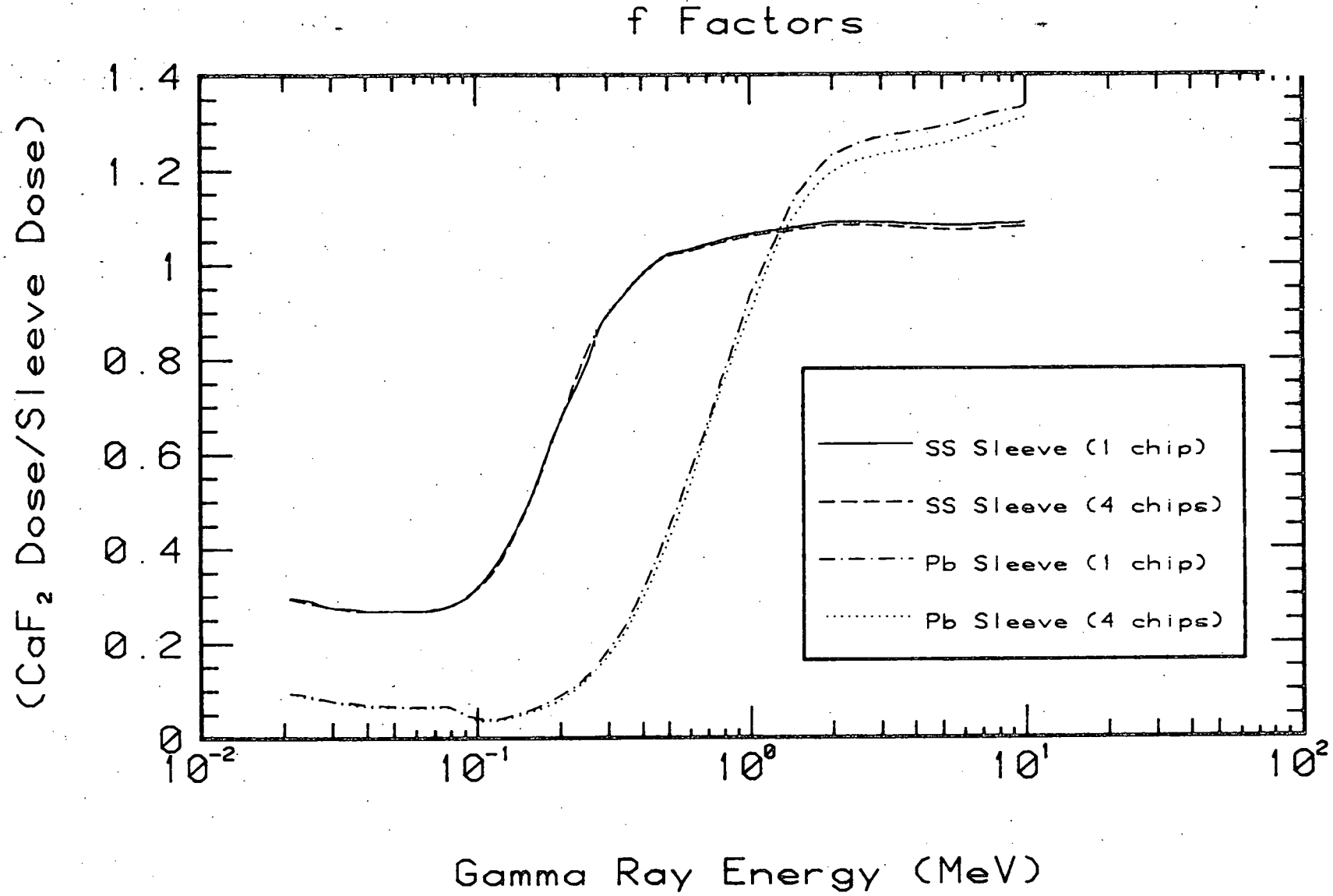


Figure C.5 : F-factors for $CaF_2$:Dy in stainless steel and lead sleeves. The difference at approximately 250 keV between the values for one or four chips in stainless steel is an artifact due to the smoothing routine in the plotting program.

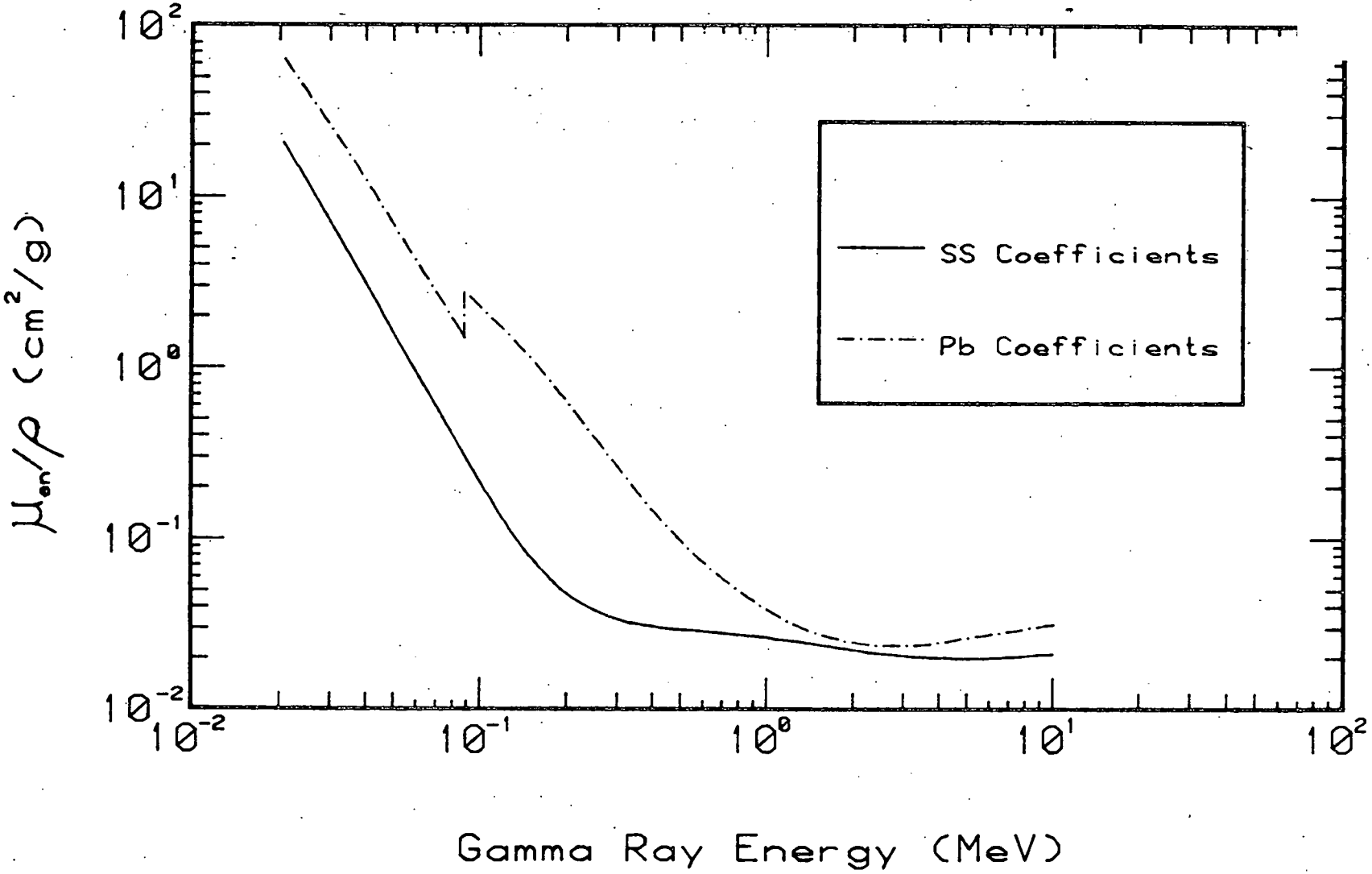


Figure C.6: Mass energy absorption coefficients in stainless steel and lead.

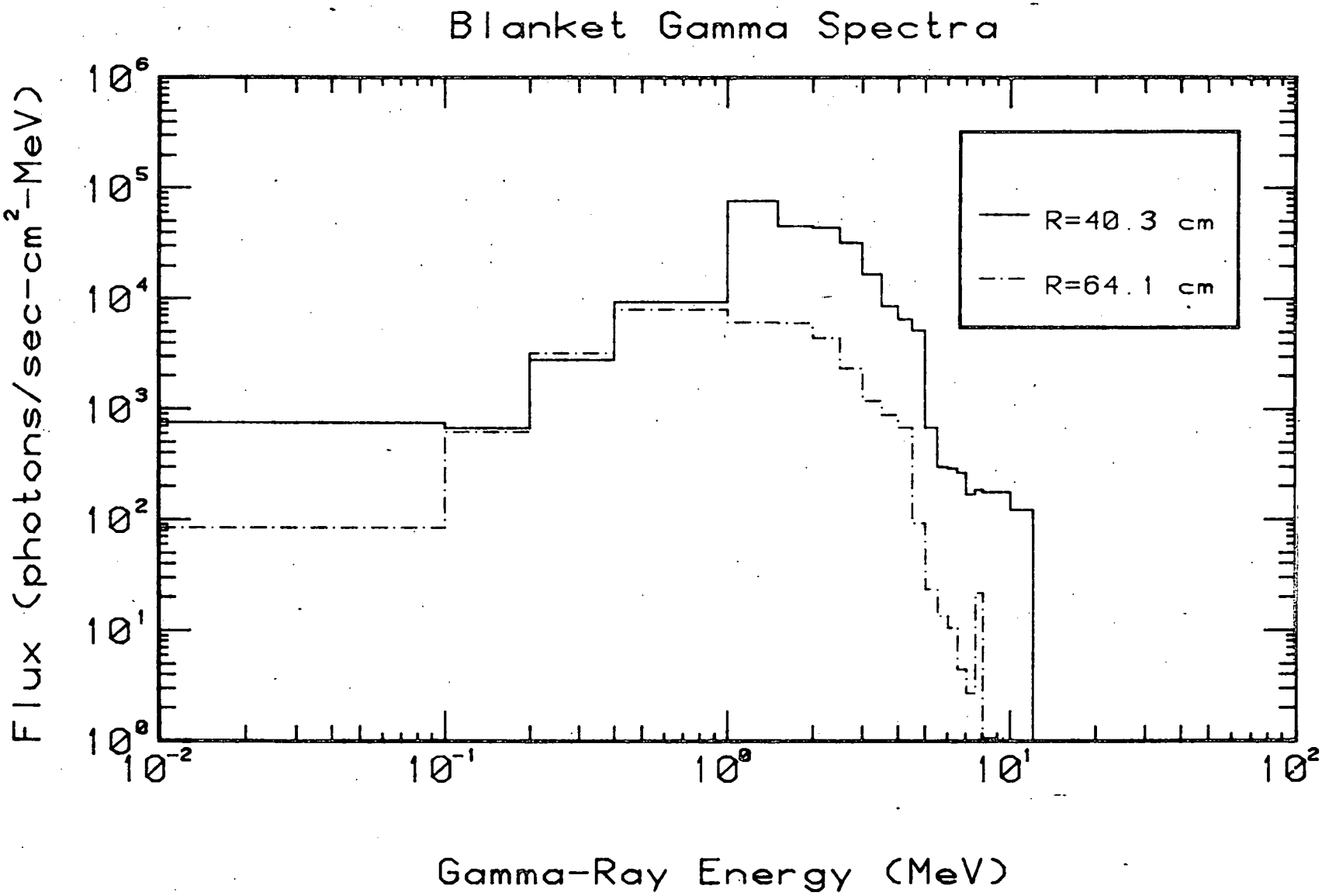


Figure C.7: Preliminary calculated gamma-ray energy spectra in the initial FBBF loading. The calculational methods given in Ref. 13 were used. Neutron absorption cross sections for uranium-238 were self-shielded in the current calculations but not in the calculations given in Ref. 13. Gamma-ray production cross sections have not yet been self-shielded.

## C.2. Installation and Testing of Facility, Facility Equipment, and Preparation of Operating Procedures

During the progress period foil activation measurements were made to verify reproducibility of foil activation data and the azmuthal symmetry of the FBBF facility. The first of these measurements were required to verify the fact that data taken at various times in the same location can be added together in order to reduce the experimental error due to counting statistics. The measurements of the azmuthal symmetry of the FBBF were made to verify one of the basic assumptions in the design criteria.

### C.2.1 Reproducibility of Foil Activation Data (G.A. Harms and F.M. Clikeman)

Because of the relatively low level of neutron fluxes in the FBBF facility, especially in the outer regions near the blanket-reflector interface, the counting statistics from single activation foils frequently do not have the precision desired for meaningful comparisons between experimental and calculated results. In order to reduce the uncertainty in the experimental measurements it was important to establish the fact that activation data from different experimental runs, activated at the same location, be added together. During the progress period two experiments were performed to verify that data from different foils, activated at different times, but in the same position can be added together.

The first experiment was performed using the $^{55}Mn(n,\gamma)^{56}Mn$ reaction. The foils were activated at various times up to 24 hours and counted for approximately two half-lives or five hours. The irradiations proceeded over a two week period at several different locations in the blanket of the FBBF facility. The measured activity of the foils were corrected for irradiation time, decay of the activity following removal from the FBBF facility, and decay of the californium source to yield a saturated activity based upon a neutron source strength of $10^{10}$ neutrons per second. The results are shown in Figure C.8. Analysis of the distribution of the data points about the mean values are consistant with the standard deviation determined from the counting statistics. The standard deviation from the manganese experiments were about 2%.

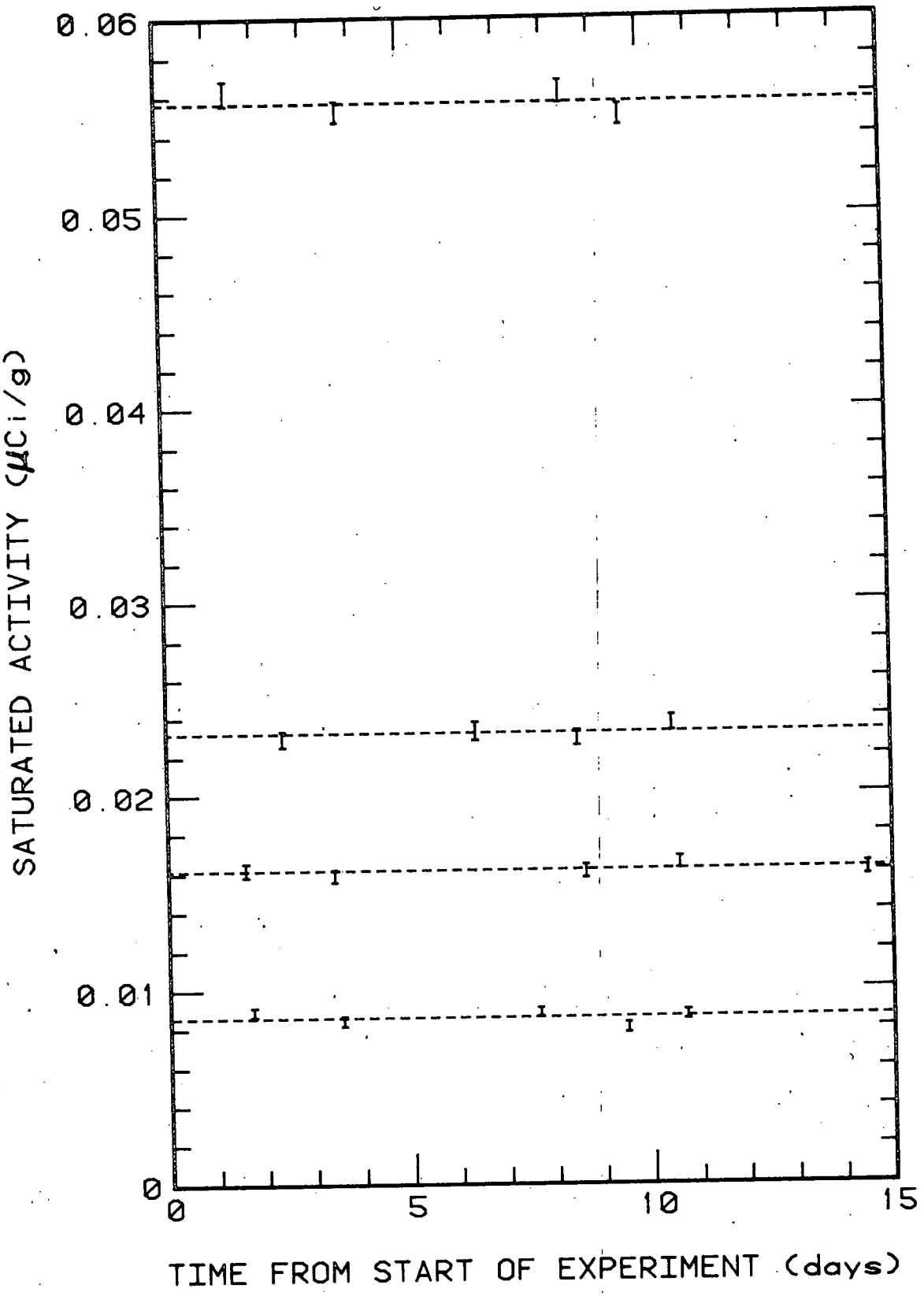


Figure C.8: Reproducibility test of the FBBF using manganese foils. The soild lines indicate the average activity at each position. The measurements were taken radially at 23.7 cm, 50.3 cm, 56.3 cm, and 71.1 cm (top to bottom) in positions 1, 10, 12, and 17 of Sector A.

A second test of the reproducibility of activation data was performed using indium foils. The series of 21 irradiations were made in position A2 (radius 26.6 cm) over a period of three days. Figure C.9 presents the results of these experiments. The data are plotted with one standard deviation error bars derived from the counting statistics. For these measurements the standard deviation was 0.85%. The average indium activity is indicated by the dashed line. Five of the 21 measurements fall more than 1 standard deviation away from the average value; 2 of these 5 values fall more than 2 standard deviation from the average consistant with statistical predictions. A chi-square analysis of the data gave a value of chi-square equal to 20 with the probability of chi-square being exceeded by another experiment being equal to 0.45. Thus, it may be concluded that random errors in the data introduced by factors other than counting statistics are small and that the data from several foil radiations may be added together to improve the precision of the measurements.

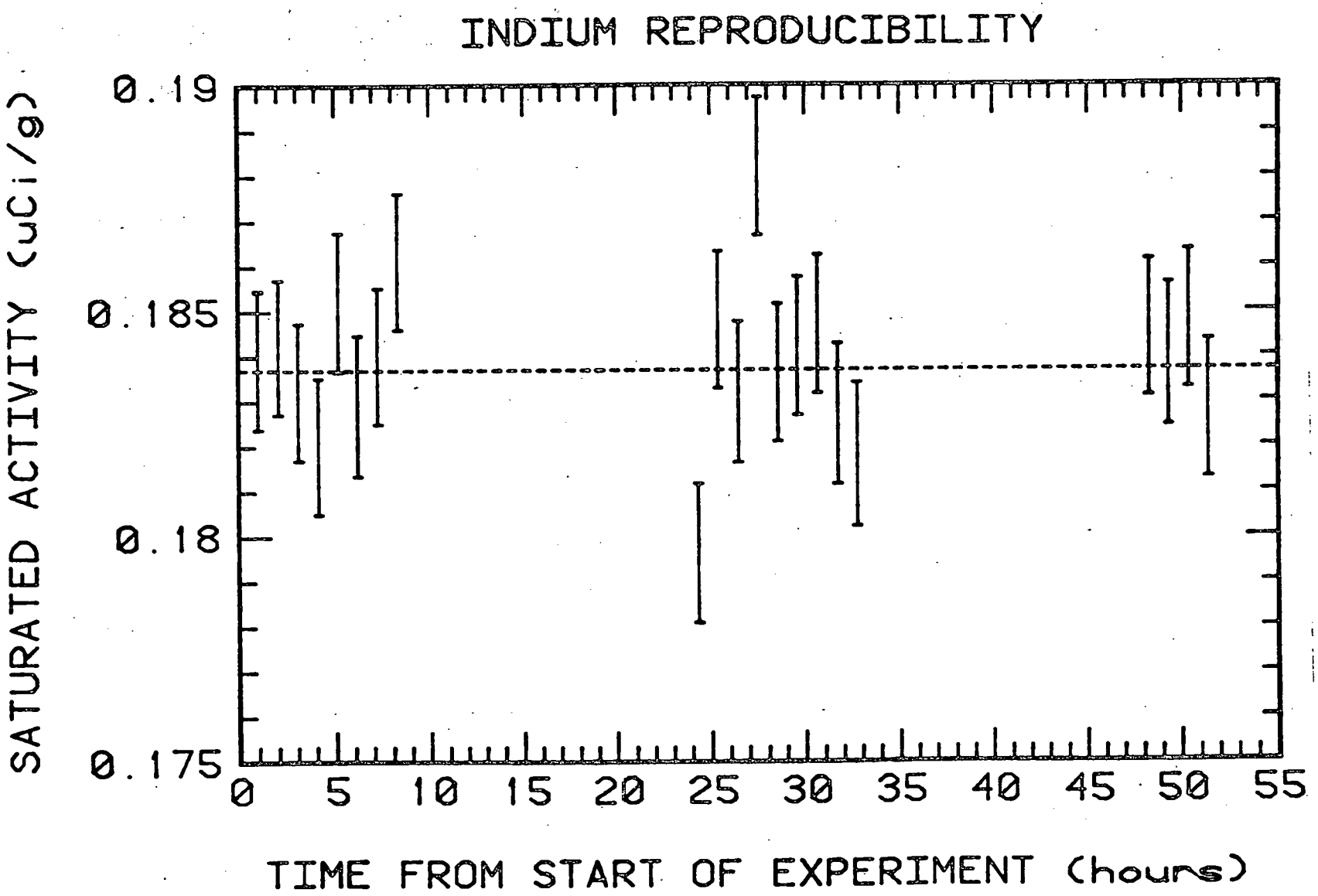


Figure C.9: Integral capture measurements for indium-115 as a function of time for position A.2. The error bars are at one standard deviation.

### C.2.2 Azmuthal Foil Irradiation
(G.A. Harms and F.M. Clikeman)

A preliminary measurement of the azmuthal symmetry of the FBBF facility made by activating gold foils was reported in the previous quarterly progress report. The preliminary measurement showed an asymmetry in the facility that can be fit by cosine distribution, cos 0/2. The maximum asymmetry at the time was 4% of the preliminary measurement one 60° sector of the FBBF facility was loaded with extra aluminum clad fuel rods making the interface between the inner stainless steel clad and the outer aluminum clad regions of the blanket at a radius of 45.15 cm. In the other five sectors of the blanket the inner face between the two regions are at a radius of 54.03 cm. Since the preliminary azmuthal traverse was taken at a radius of 32 1/2 cm it was assumed that the observed day symmetry was caused by the perturbation introduced by the additional aluminum especially since the position of the highest gold activity corresponded with the center of the aluminum sector. Subsequently during the progress period the perturbation was removed and the azmuthal gold measurements were repeated. The second seris of azmuthal measurements, repeated with a uniform blanket, again showed the same asymmetry as shown in Figs. C.10 and C.11. Again the magnitude of the asymmetry is about 4%. Additional measurements both axial and radial are being conducted at this time to investigate the causes with the observed asymmetry.

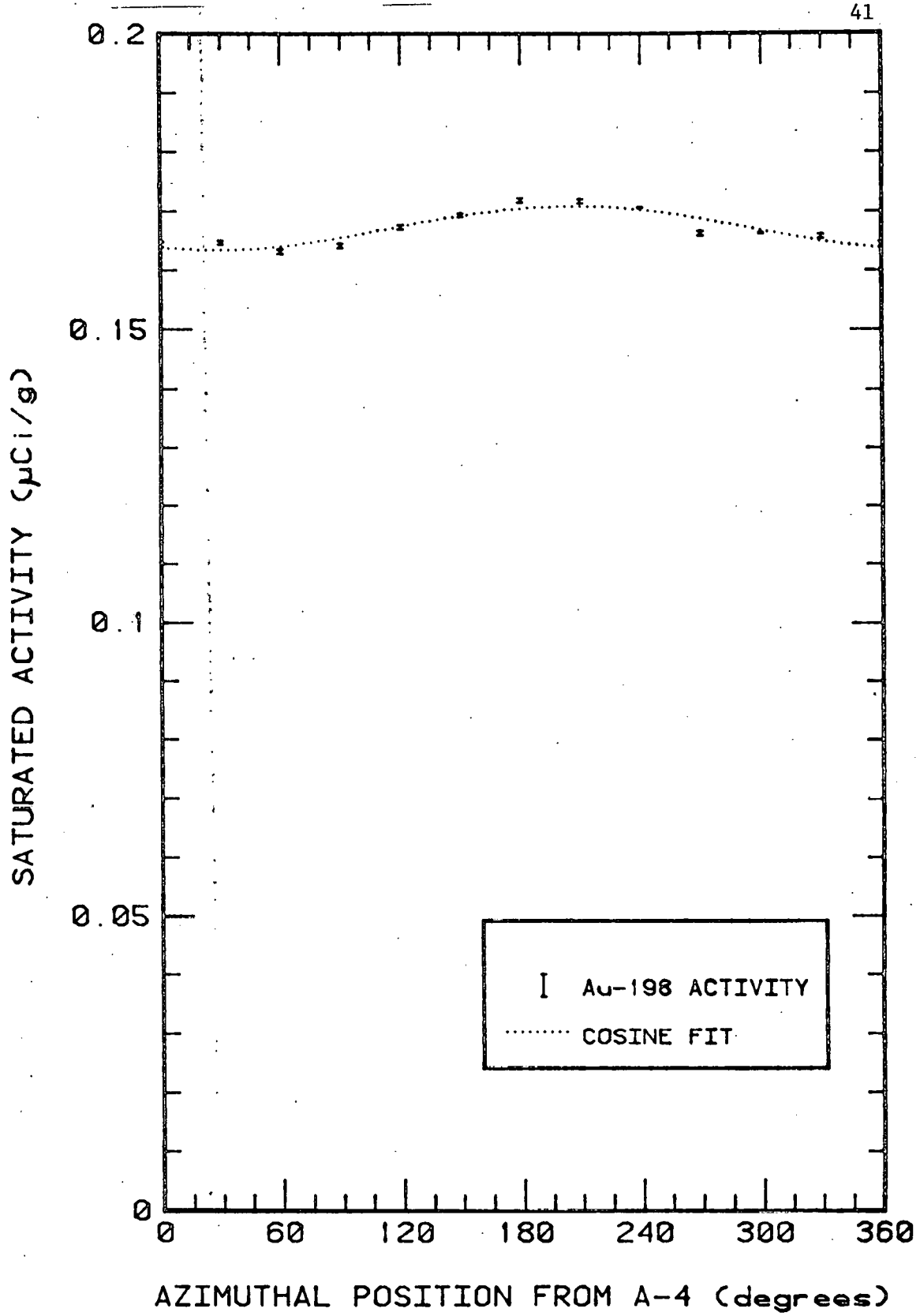


Figure C.10: Gold capture rates as a function of azmuthal position from the center of sector A. The error bars are shown at one standard deviation. The curve is a cosine fit of the experimental data.

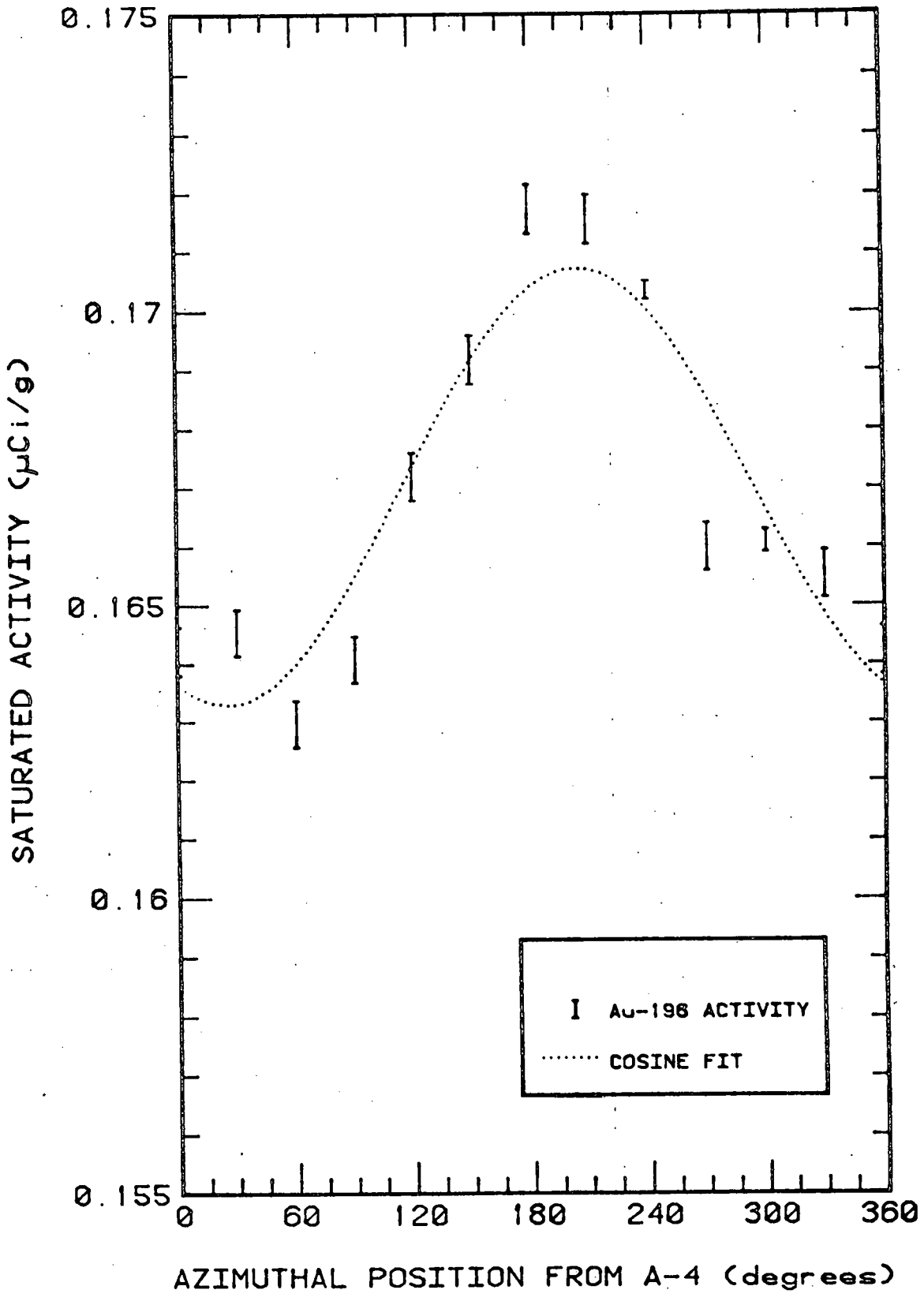


Figure C.11: Gold capture rates as a function of azmuthal position from the center of sector A, zero suppressed. The error bars are shown at one standard deviation. The curve is a cosine fit to the experimental data.

## C.3. Experimental Measurements Using the FBBF Facility

During the progress period a number of neutron capture reaction rates were measured as a function of radius throughout the blanket regions of the FBBF facility. Results of these measurements together with comparisons with calculations are reported in the following sections.

### C.3.1. Uranium-238 Neutron Capture Rate Measurements (G.A. Harms and F.M. Clikeman)

The U-238 neutron capture reaction rate has been investigated as a function of radial position thoughout the blanket of the FBBF facility. Nine depleted (less than 400 ppm) uranium foils were irradiated over the course of three weeks and counted for the NP-239 activity. Each foil was irradiated for 120 hours and then removed and allowed to decay five hours before counting. The decay allowed for all of the U-239 to decay to NP-239 before the start of the analysis. Each foil was then counted for either 24 or 48 hours depending on its location in the FBBF and its level of activity. Although three gamma-rays from the decay of the NP-239 were detected and analyzed only the information from the 277 keV peak were used in the final comparisons with calculations. Both of the other two gamma peaks are known to contain gamma-rays from fission products produced by either the fission reaction in U-238 or the small remaining quantity of U-235 in the foils. The activities were corrected for the half life decay of neptunium, the detector efficiency, the foil weight, the californium source decay, and normalized to a source strength to $10^{10}$ neutrons per second. The results of the neptunium activity verses radial position are shown in Fig. C.12. Also shown on the plot are two calculations, one using the 2DB computer code and the 30 neutron group cross sections described in Section B.2. The second calculation was made using the ANISN[14] computer code and a 23 group neutron cross section. The cross sections for both computer codes were self-shielded for 300° K. The comparison shows that although the shape of the calculated

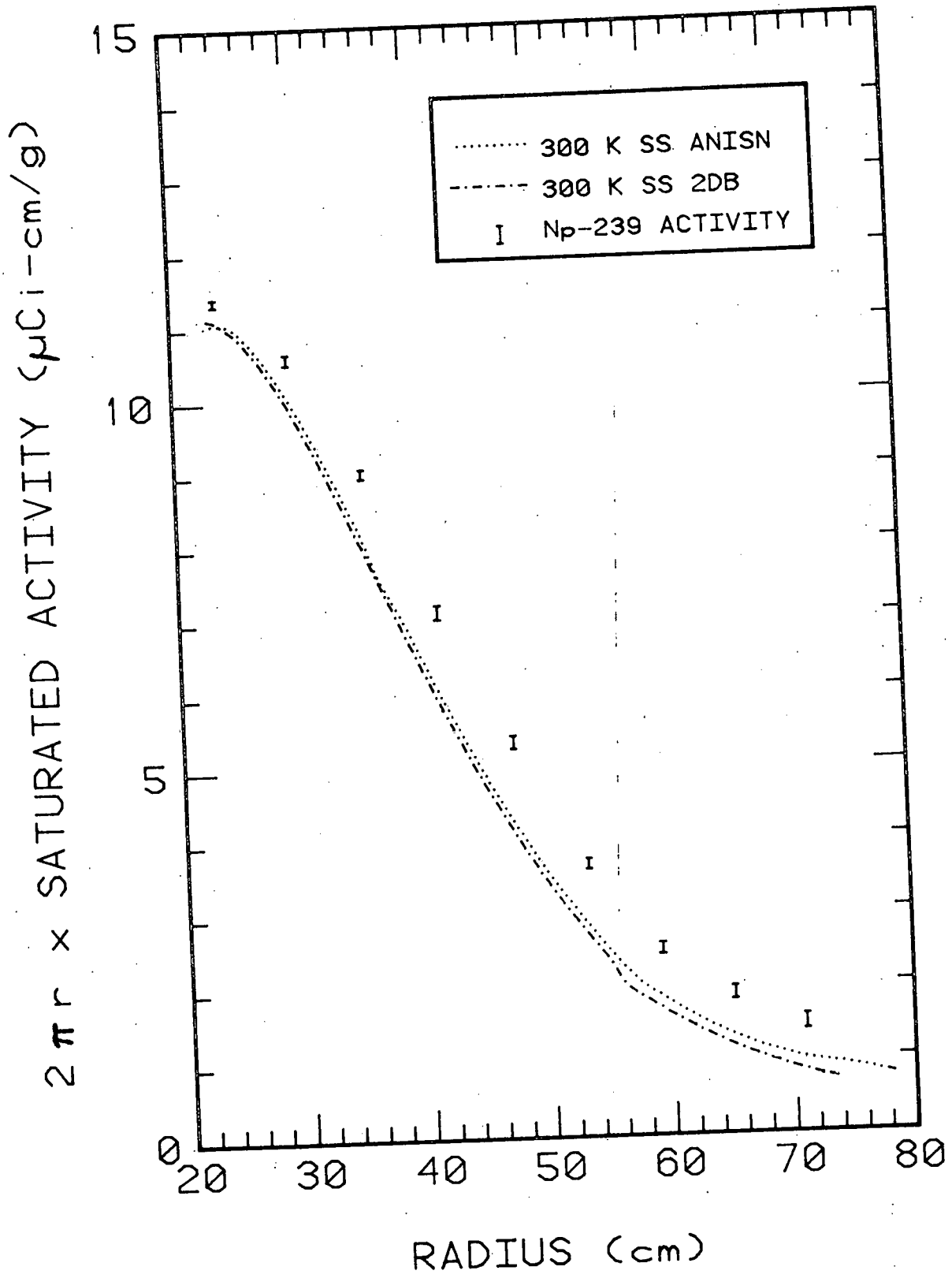


Figure C.12: Integral uranium-238 capture rates. The two curves are 2DB and ANISN calculations with cross sections self-shielded at 300°K. The error bars on the experimental data are at one standard derivation and are due only to counting statistics.

values agree well with each other and the general shape agrees well with experimentally measured data points the calculated values consistently underpredict the experiment. Both the experimental data points and the calculated curve are corrected to a neutron source strength of $10^{10}$ neutrons per second. No other normalizations have been made to make the values agree.

### C.3.2. Measurements of the $^{197}An(n,\gamma)^{198}Au$ Reaction (G.A. Harms, M.P. Sohn and F.M. Clikeman)

The preliminary gold neutron capture reaction rates measurements have been repeated. The gold foils were irradiated for 60 hours and then analyzed by counting the 411 keV gamma-ray to determine the activity of each foil. After preliminary measurements had indicated that no competing reactions were taking place in the gold foils, the foils were counted using a 3 in x 3 in well type NaI(tℓ) scintillation detector (see Sec. C.1.1). The results of the measurement as a function of a radial position are shown in Fig. C.13 together with a calculation made using the 2DB computer code and a 30 group cross section self-shielded for 300° K. The graph shows good agreement between the measured integral reaction rates and the calculation. Again, the experimental data and the calculated values have been corrected to an absolute source strength of $10^{10}$ neutrons per second rather than trying to normalize the curves for a best fit. Figures C.14 through C.17 show the calculated differential neutron capture rate for gold as a function of position throughout the blanket. It is noteworthy to see how the various neutron groups responsible for activity of the gold shift from higher energies to lower energies and how the strong resonance in the gold neutron capture cross section becomes dominate at the lower neutron energies in the outer regions of the blanket. The change in the shape of the differential capture rates as a function of position throughout the blanket together with the close match of the integral reaction rates as the function of position as shown in Fig. C.13 generates confidence in the ability of

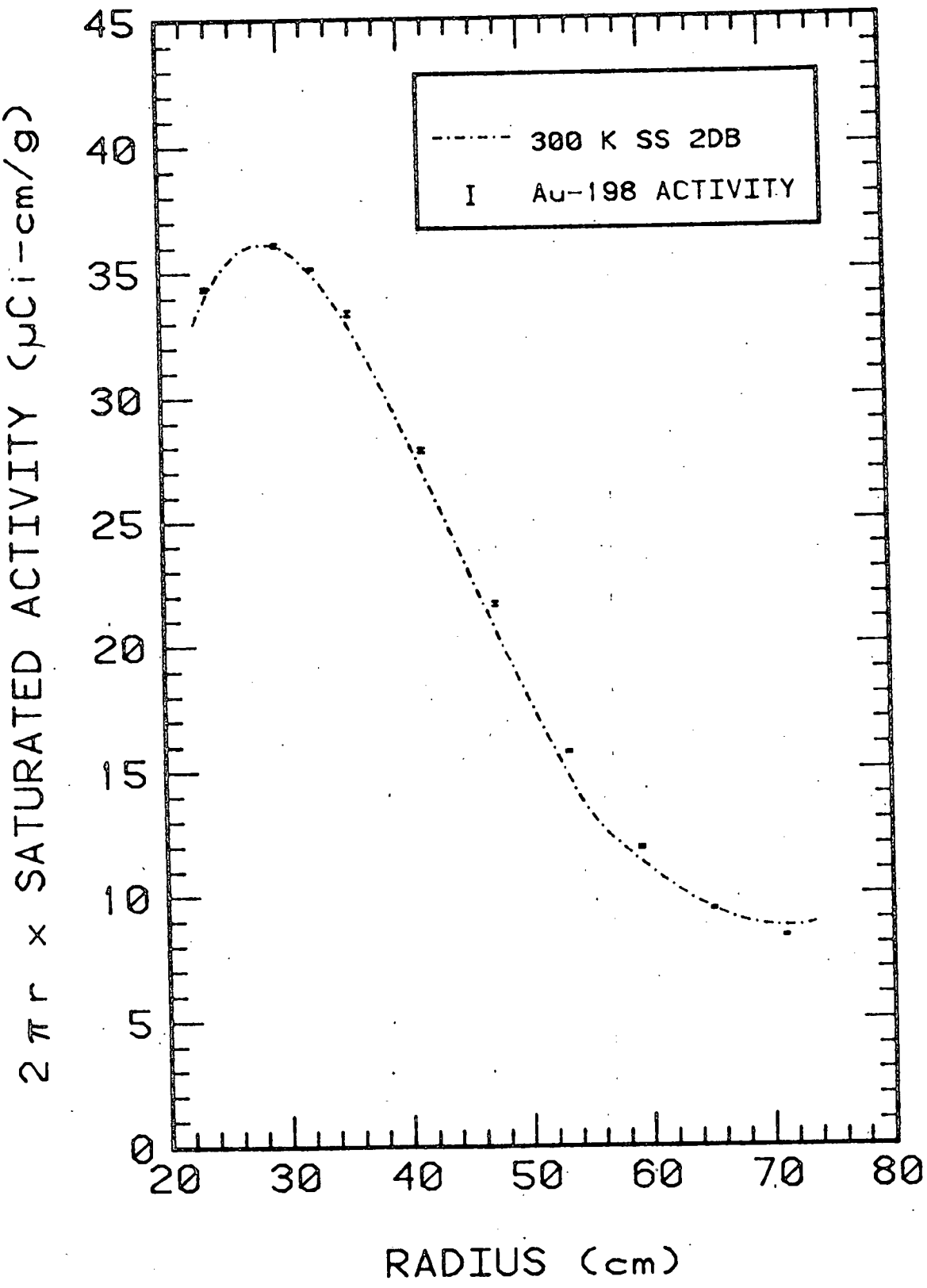


Figure C.13: Integral gold capture rates. The curve shows the results of a 30-group diffusion calculation using 2DB. The experimental error bars are at one standard deviation and account only for errors in counting statistics.

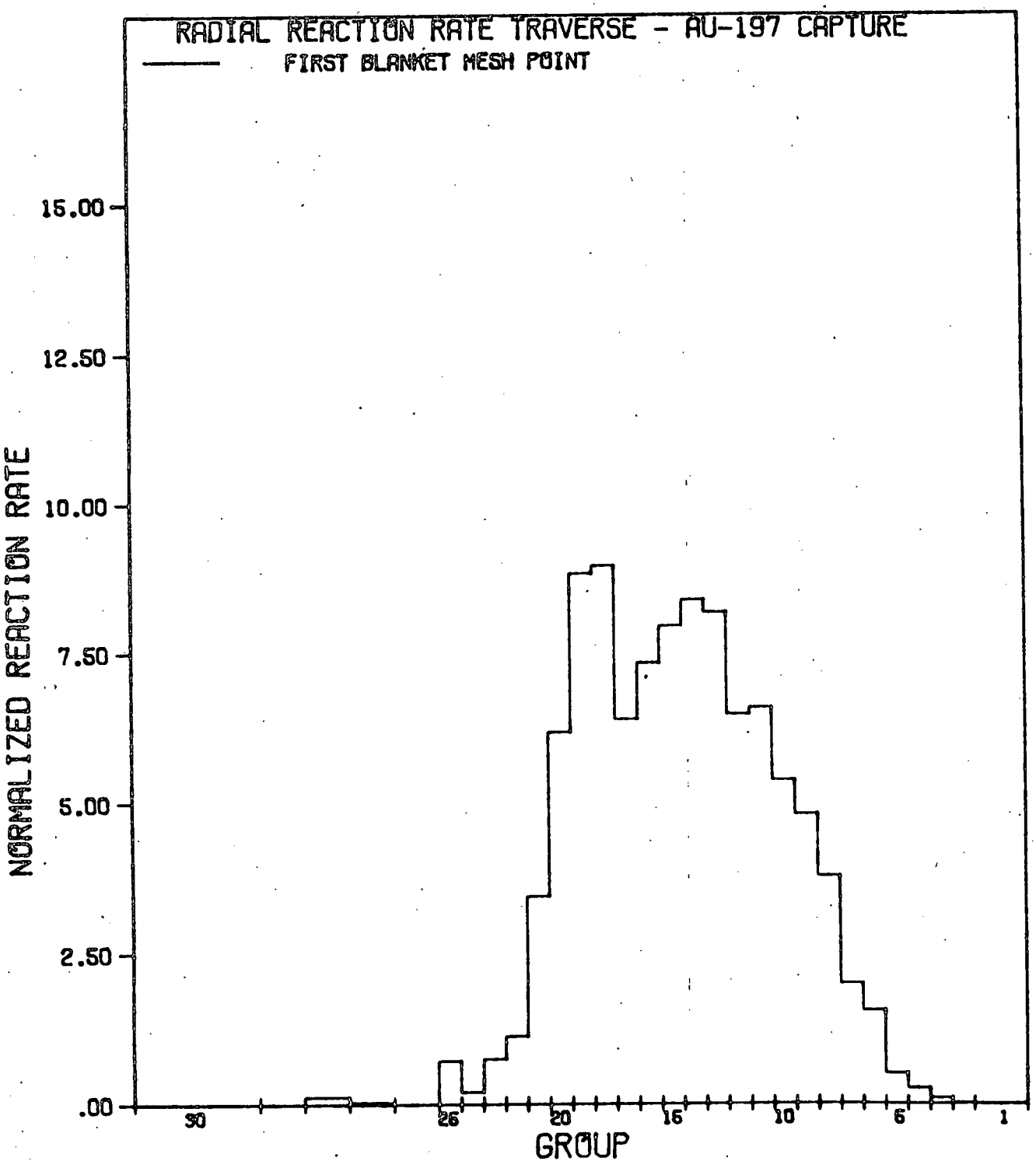


Figure C.14: Differential capture rate for gold at 23.7 cm., calculated using 2DB with a 30 group, self-shielded (300°K) cross section set.

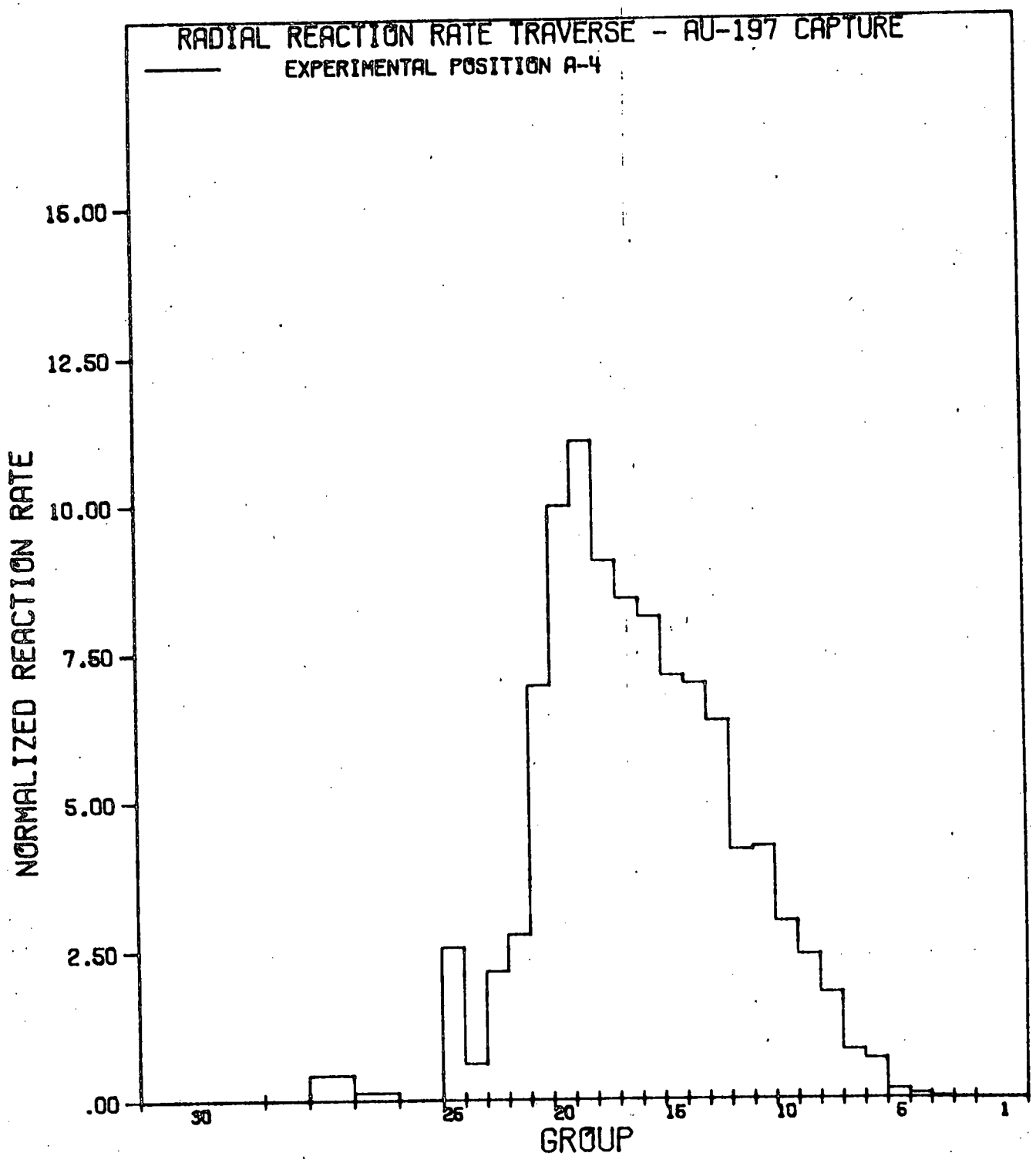


Figure C.15: Differential capture rate for gold at 38.5 cm., calculated using 2DB with a 30 group, self-shielded (300°K) cross section set.

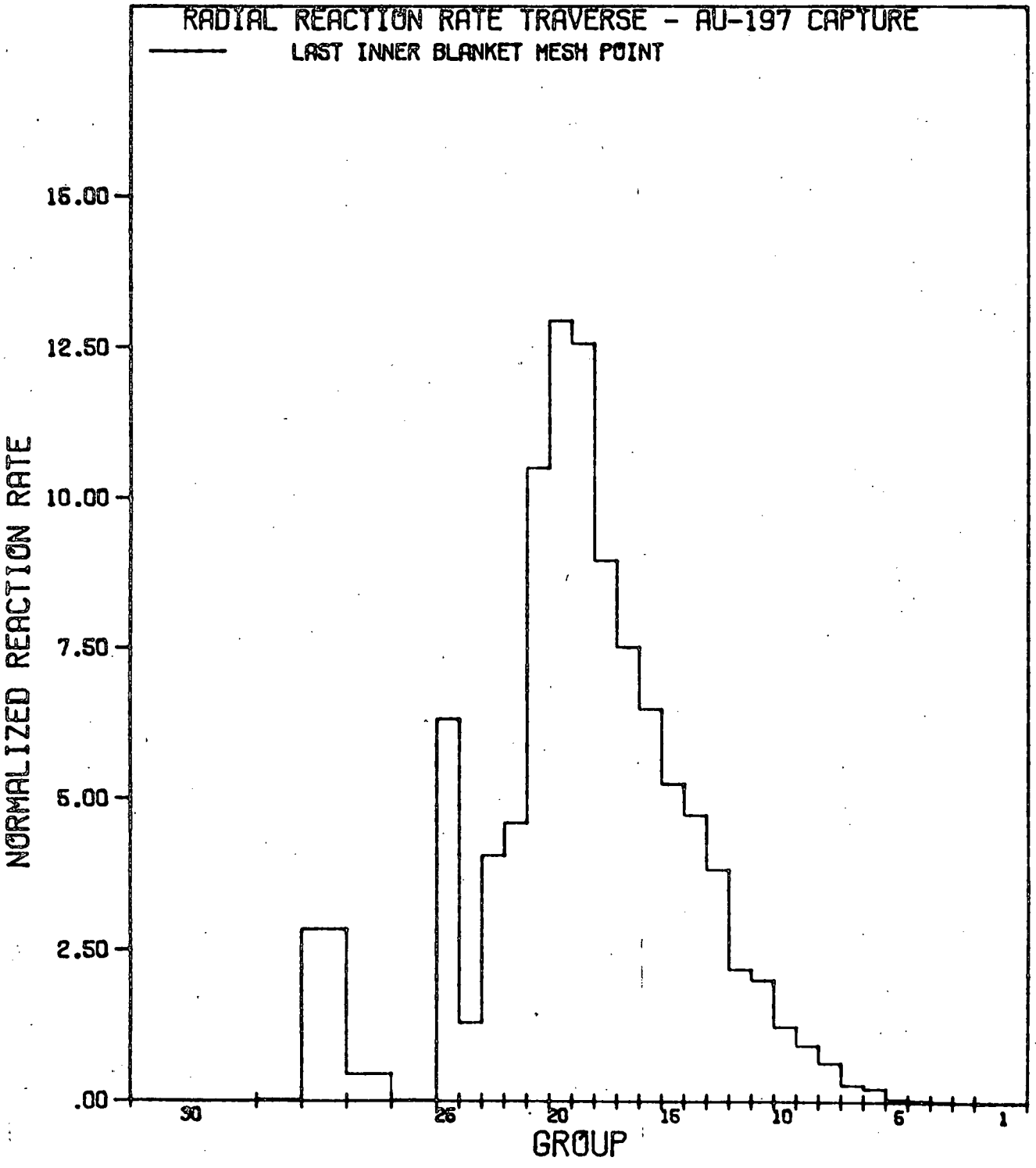


Figure C.16: Differential capture rate for gold at 56.3 cm, calculated using 2DB with a 30 group, self-shielded (300°K) cross section set.

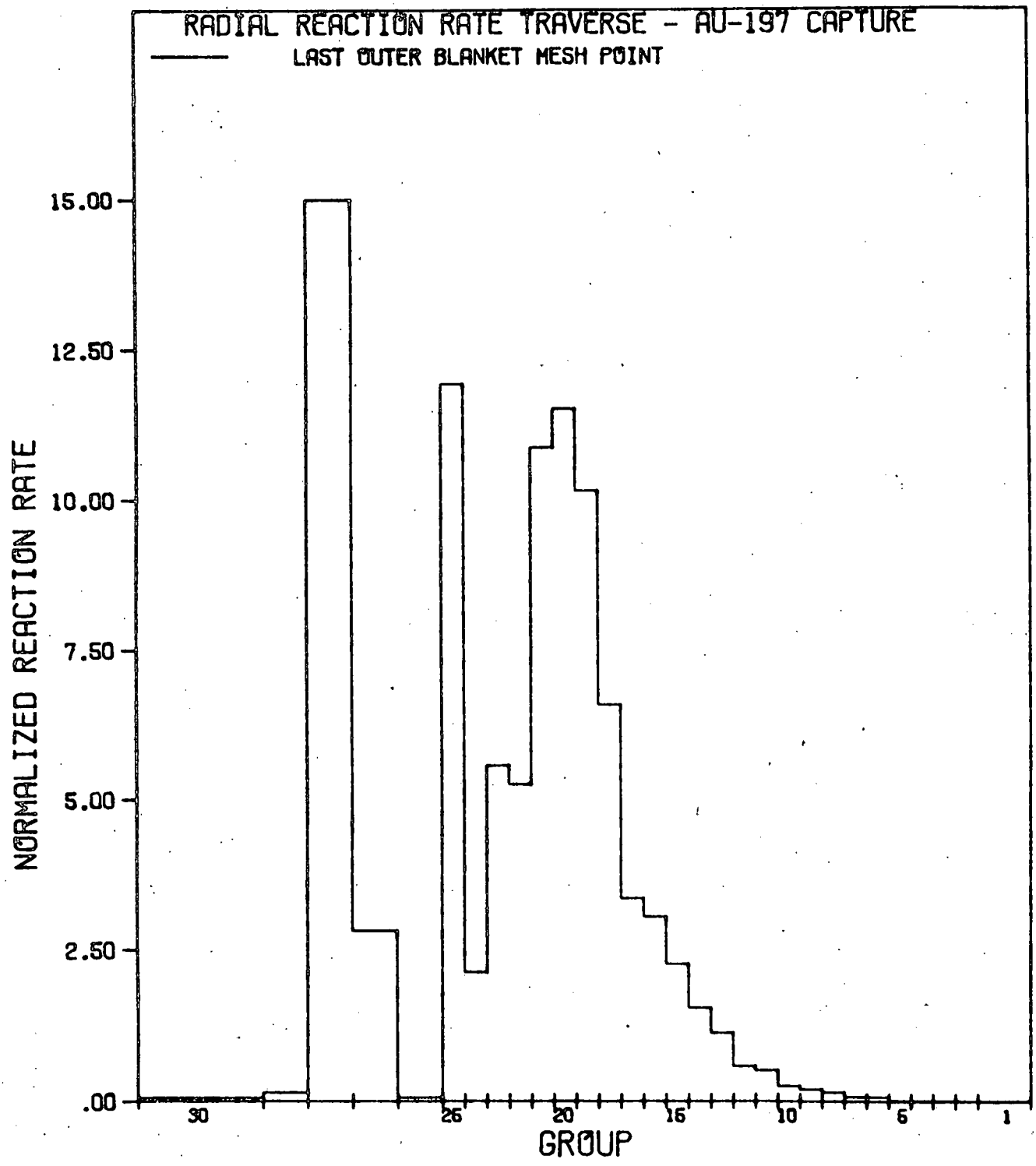


Figure C.17: Differential capture rate for gold at 71.1 cm.,calculated using 2DB with a 30 group, self-shielded (300°K) cross section set.

the computer code 2DB to accurately calculate the neutron reaction rates in the blanket. However, the lack of agreement between the calculated values and experimental results for the U-238 neutron capture rate indicate that additional work must still be done. Experiments are now being planned to measure the integral reaction rates for a varity of other reactions in order to determine whether the lack of agreement between the calculated and experimental values for the U-238 reaction are caused by the computer code or by the evaluated cross section set.

## REFERENCES


1. I.I. Bondarenko, Ed., Group Constants for Nuclear Reactor Calculations (Consultants Bureau, New York 1964).

2. R.B. Kidman, R.E. Schenter, R.W. Hardie, and W.W. Little, "The Shielding Factor Method for Generating Multigroup Cross Sections for Fast Reactor Analysis," Nucl. Sci. and Eng. 48, 189 (1972).

3. R.W. Hardie and W.W. Little, Jr., "1DX, A One-Dimensional Diffusion Code for Generating Effective Nuclear Cross Sections," Battelle Northwest Laboratory report BNWL-954 (1969).

4. R.B. Kidman and R.E. MacFarlane, "LIB-IV, A Library of Group Constants for Nuclear Reactor Calculations," Los Alamos Scientific Laboratory report LA-6260-MS (1970).

5. R.E. MacFarlane and R.B. Kidman, "LINX and BINX: CCCC Utility Codes for the MINX Multigroup Processing Code," Los Alamos Scientific Laboratory report LA-6219-MS (1976).

6. R.B. Kidman and R.E. MacFarlane, "CINX: Collapsed Interpretation of Nuclear X-Sections," Los Alamos Scientific Laboratory report LA-6287-MS (1976).

7. B.M. Carmichael, D.A. Meneley, and D.R. Vondy, "Report of the Subcommittee of Standard Interface Files, Prepared for the Committee on Computer Code Coordination," Los Alamos Scientific Laboratory report LA-5324-MS (1973).

8. W.W. Little, Jr., and R.W. Hardie, "2DB User's Manual -- Revision 1," Battelle Northwest Laboratory report BNWL-831 REV1 (1969).

9. Fast Breeder Blanket Facility Progress Report for the Period January 1 - March 31, 1978, PNE-78-128, COO-2826-8, Purdue University, West Lafayette, Indiana.

10. K.R. Koch and F.M. Clikeman, "Gamma-Ray Dosimetry Measurements Using TLD Dosimeters," FBBF Quarterly Progress Report for the Period April 1, 1978 - June 30, 1978, pp. 21-22, COO-2826-9, PNE-78-128, Purdue University, West Lafayette, Indiana.

11. G.G. Simons, Kansas State University, Private Communication (1978).

12. G.G. Simons and L.L. Emmons, "Experimental Evaluation of a Model for Calculating the Gamma-Ray Response of Encapsulated Solid-State Dosimeters," Argonne National Laboratory, ZPR-TM-238 (1976).

13. R.H. Johnson and J.H. Paczolt, "Coupled Neutron-Gamma-Ray Transport Calculations for Initial FBBF Loading," FBBF Quarterly Progress Report for the Period January 1, 1978 - March 31, 1978, pp. 19-28, COO-2826-8, PNE-78-132, Purdue University, West Lafayette, Indiana.

14. W.W. Engle, Jr., "A User's Manual for ANISN, A One Dimensional Discrete Ordinates Transport Code with Anisotropic Scattering" Union Carbide Corporation K-1693 (1967).